AMERICAN UNIVERSITY OF BEIRUT

RELIABILITY-BASED STRUCTURAL DESIGN

of RETAINING WALLS SUPPORTING

SPATIALLY VARIABLE SOILS

by
BATOUL AHMAD TARHINI

A thesis
Submitted in partial fulfillment of the requirements
for the degree of Master of Engineering
to the Department of Civil and Environmental Engineering
of the Maroun Semaan Faculty of Engineering and Architecture
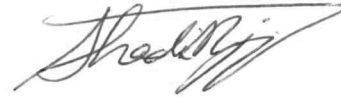at the American University of Beirut

Beirut, Lebanon
August 2019

AMERICAN UNIVERSITY OF BEIRUT

RELIABILITY-BASED STRUCTURAL DESIGN

OF RETAINING WALLS SUPPORTING SPATIALLY VARIABLE

SOILS

by
BATOUL AHMAD TARHINI

Approved by:

_____

Dr. Shadi Najjar, Associate Professor   Advisor
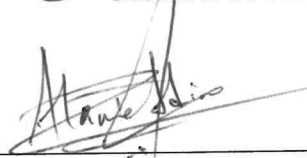Department of Civil and Environmental Engineering

_____

Dr. Salah Sadek, Professor   Member of committee
Department of Civil and Environmental Engineering

_____

Dr. Ibrahim Alameddine, Assistant Professor   Member of committee
Department of Civil and Environmental Engineering

Date of thesis/dissertation defense: [August 20, 2019]

AMERICAN UNIVERSITY OF BEIRUT

THESIS, DISSERTATION, PROJECT RELEASE FORM

Student Name:____Tarhini_____Batoul_____Ahmad_____

                 Last   First   Middle

⊘ Master's Thesis   ◯ Master's Project   ◯ Doctoral Dissertation

[✓]   I authorize the American University of Beirut to: (a) reproduce hard or electronic copies of my thesis, dissertation, or project; (b) include such copies in the archives and digital repositories of the University; and (c) make freely available such copies to third parties for research or educational purposes.

[ ]   I authorize the American University of Beirut, to: (a) reproduce hard or electronic copies of it; (b) include such copies in the archives and digital repositories of the University; and (c) make freely available such copies to third parties for research or educational purposes after:

One ---- year from the date of submission of my thesis, dissertation, or project.
Two ---- years from the date of submission of my thesis, dissertation, or project.
Three ---- years from the date of submission of my thesis, dissertation, or project.

Signature _____   Date September 12 , 2019

ACKNOWLEDGMENTS

AN ABSTRACT OF THE THESIS OF

Batoul Ahmad Tarhini   for   Master of Engineering
                                           Major: Geotechnical Engineering

Title: Reliability-based structural design of retaining walls supporting spatially variable soils

The design of retaining walls is affected by spatial variability in the properties of the retained backfill and the foundation soil. In practice, the conventional approach for designing retaining walls is deterministic in nature and is based on ensuring acceptable design factors of safety for different limit states of wall failure. The only exception is the design method that is available in Eurocode 7, where partial load and resistance factors have been recommended to ensure a target level of safety in the design. Although these codes are considered to include the uncertainties in the design load and capacity, the recommended partial safety factors may not realistically incorporate the impact of spatial variability in the properties of the supported backfill and foundation soil on the design, since the calibration studies that were conducted to determine the safety factors were not based on realistic random field modeling of the soils involved. In addition, existing reliability-based design approaches for retaining walls focus on the failure in the soil and do not include design aspects of the structural behavior of the wall. The main objective of this thesis is to quantify the level of risk associated with the design of a cantilever retaining wall using the conventional deterministic design approaches and approaches that are based on partial factors of safety (ex. Eurocode 7). The objective will be attained by utilizing random fields that represent the variability in the backfill and foundation soils in the finite difference software FLAC 2D®. The effect of the properties of the random field on the design of the retaining wall will then be investigated to provide recommendations that would aid the design of cantilever walls supporting cohesionless backfill.

CONTENTS

Chapter

ILLUSTRATIONS

TABLES

CHAPTER 1

INTRODUCTION

1.1   Backgound

In the traditional design approaches for retaining walls, the earth pressure distribution that is needed in design is generally evaluated using the Rankine, Coulomb, or Lancelotta earth pressure theories, which simplistically assume that the backfill soil is homogeneous and that the foundation soil that supports the wall is infinitely rigid. In these approaches, every mode of failure (limit state) is examined separately to ensure target factors of safety against the particular limit state. Eurocode 7 replaced the traditional factor of safety approach by the partial factor of safety approach, whereby select/appropriate factors are used to reduce the strength/resistance parameters and to increase the applied load. The partial safety factor approach is expected to provide a more realistic design risk against the different limit states considered.

Recently, various fields in geotechnical engineering (ex. slope stability, foundation design, and retaining systems) have been tested/affected by random field modeling, whereby the soil is modeled as a random field in the context of finite element or finite difference software packages. These studies have highlighted the importance of modeling the spatial variability of the soils as random fields with predetermined realistic spatial correlation structures, rather than simple random variables. These studies showed that traditional design factors of safety may not always lead to acceptable levels of risk in the design for particular spatial correlation structures. In addition, results obtained by Goh et al. (2009) showed that the partial safety factor approach used in Eurocode 7 cannot be reliably used to ensure target levels of risk for all cases of soil variability.

They showed the need for a fully probabilistic design approach which models all the sources of uncertainty in the problem and develop a direct linkage between uncertainties in the design variables and the probability of failure.

This study is devoted to investigating the effect of spatial variability of soil properties on the structural design of walls using the random finite difference method implemented by FLAC 2D®. The backfill soil will be assumed to be a cohesionless sand and the foundation soil will be modelled as a stiff/dense material. Both soils will be modeled using random fields.

1.2   Objectives and scope of research

An investigation of the previous work on retaining walls points to the importance of the effect of spatial variability of soil properties on the geotechnical limit states for design. Moreover, most of the published studies simulate the properties of the backfill soil using random variables rather than true random fields. They study the stability of walls and the probability of failure without investigating the effect of the spatial variability of the properties of the backfill soil on the structural behavior of the wall (moments, deflection, steel reinforcement etc.).

The main purpose of this thesis is to conduct a probabilistic analysis to accomplish the following goals: (1) quantify the risk level that is inherent in cantilever retaining wall designs that are based on deterministic approaches or partial safety factor approaches (Eurocode 7), (2) study the sensitivity of the inherent risk levels to the different parameters involved such as mean value, coefficient of variation, and spatial correlation structure of the soil properties under and behind the retaining wall, and (3) propose/recommend changes to the partial safety factors in Eurocode 7 to produce designs with a consistent and realistic target probability of failure.

To reach the goals mentioned above, the following steps are needed:

1. Conduct a literature review that focuses on the studies that relate to the reliability based design of retaining walls supporting cohesionless backfill. This includes conducting a literature review on the applications of retaining systems that are modeled using FLAC 2D and the method used to design a cantilever retaining wall according to Eurocode.

2. Design a cantilever retaining wall according to Eurocode using traditional methods.

3. Create a procedure to conduct Monte Carlo Simulations for retaining walls using soil properties that are modeled using random fields (using R software) and transport these realizations to FLAC 2D to run the stability analyses.

4. Conduct a parametric study to quantify the effect of varying certain parameters such as the mean, the COV, and the correlation lengths of the random field describing the soil properties of the backfill and the foundation soil.

CHAPTER 2

LITERATURE REVIEW

The design of different types of retaining walls using probabilistic approaches that take into consideration the variability of soil properties has been addressed by many researchers in the literature. The following is a review of some of these works:

2.1   Studies involving the reliability based design of retaining walls:

Chalermyanont et al. (2005) used Monte Carlo simulations to study the effect of variability in soil properties on the probability of external failure of Mechanically Stabilized Earth (MSE) walls where they considered three types of failure: overturning, bearing capacity, and sliding. A second analysis was done to assess the internal stability of MSE walls taking into account the spatial variability of the soil, within a practical reliability-based design procedure.

In order to simulate the spatial variability of soil properties, the authors divided the foundation and the backfill into a series of cells, where the soil properties are uncorrelated. The factor of safety was calculated using traditional methods. The results related to the sliding mode of failure indicated that the coefficient of variation (COV) and the mean of the backfill internal friction angle have a significant effect on the probability of failure. On the other hand, with reference to the overturning mode of failure, the unit weight was found to also have a significant effect. For bearing capacity considerations, the mean and COV of both the backfill and foundation soils governed the probability of failure. Chalermyanont et al. (2005) developed charts that display the required MSE reinforcement corresponding to a target probability of failure.

Sivakumar and Basha (2008) conducted a parametric study to investigate 10

4

modes of failure for cantilever retaining walls. They showed that the most sensitive

parameter is the internal angle of friction of the backfill. The authors proposed an

optimization method that could be used to determine the required wall proportions

according to the reliability Index and uncertainty in design parameters.

Goh et al. (2009) proposed a risk-based approach to study the effect of the

design equation uncertainties and the uncertainty in the geotechnical soil variables on

the design of cantilever retaining walls in sand, using the "partial factor of safety on

shear strength" approach. They assumed five lognormally distributed and uncorrelated

variables: the surcharge, soil friction angle, unit weight, applied moment, and wall

height. This was the first study which integrated a random model error that accounts

for the errors from model idealizations in the analyses.

The results (Figure 1) showed that a fixed partial factor of safety cannot be

used for all degrees of uncertainty in the soil friction angle, and that the factor of safety

recommended in several codes (between 1.2-1.25) can be used to yield designs with a

1% probability of failure, only for the cases involving a friction angle with a standard

deviation STD that is less than 2 degrees.

m_ϕ (degrees)	SD_ϕ (degrees)	FS_ϕ	
		$P_f=1\%$	$P_f=0.1\%$
30	2	1.20	1.30
	3.5	1.30	1.45
	5	1.40	1.60
35	2	1.20	1.35
	3.5	1.30	1.45
	5	1.40	1.60
40	2	1.25	1.35
	3.5	1.35	1.45
	5	1.45	1.60
45	2	1.25	1.40
	3.5	1.35	1.50
	5	1.45	1.60

Figure 1. Partial Factor Corresponding to Target Pf of 1 and 0.1% (Goh et al. 2009)

Zevgolis and Bourdeau (2010) introduced a methodology to analyze

reinforced concrete cantilever walls using a probabilistic approach. This analysis took into consideration the dependency between the failure modes by using the correlation among different parameters. The analysis was performed using Monte Carlo simulations and the properties of the backfill (unit weight and friction angle) were considered random variables that follow a beta distribution. The length of the heel of the wall was used as a variable design parameter, where the analysis was performed for heel lengths between 1.5 and 3.5 m.

Zevgolis and Bourdeau found that the factor of safety against sliding and bearing capacity failure increases linearly with increasing heel length, whereas it increases non-linearly for eccentricity (eccentricity< Base width/6) (Figure 2). In addition, they found that a higher degree of uncertainty is obtained for the bearing capacity mode of failure and that the pairs of factors of safety of sliding – overturning and sliding – bearing are highly correlated. The results also showed that assuming an independence between modes of failure will overestimates optimum heel length.
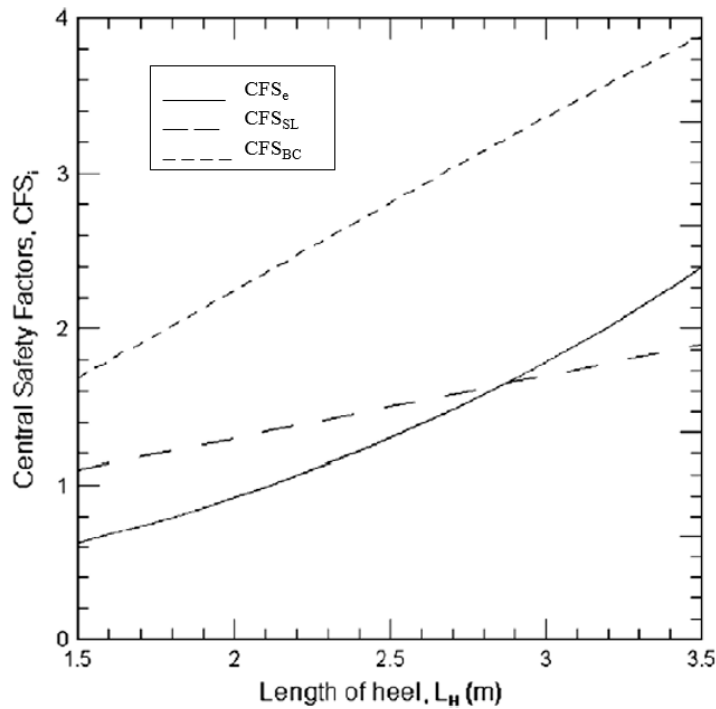
Figure 2. Length of Heel vs Factor of Safety (CFS_e: factor of safety for eccentricity, CFS_{SL}: factor of safety for sliding, and CFS_{BC}: factor of safety for bearing capacity (Zevgolis and Bourdeau 2010)

Sujith et al. (2011) utilized the first order reliability method (FORM), second-order reliability method (SORM) and Monte Carlo simulation (MCS) to calculate the probability of failure in the sliding mode for cantilever retaining walls with heights of 4, 6 and 8 m. They considered five random variables: unit weight of backfill soil, unit weight of concrete, the angle of internal friction of the soil, applied surcharge, and the coefficient of friction between the concrete and the soil. The effect of the various parameters on the probability of failure was expressed by a 'sensitivity factor'.

The results showed that the most relevant random variable is the internal friction (φ) followed by the concrete-soil coefficient of friction, and that the value of the probability of failure is identical for the three methods (Figure 3).

	h = 4 m		h = 6 m		h = 8 m	
	β	P_f	β	P_f	β	P_f
FORM	1.8415	0.0327	1.8192	0.0344	1.8487	0.0322
SORM	1.8522	0.0319	1.8296	0.0336	1.8570	0.0316
Monte Carlo simulations (5 millions)	–	0.0320	–	0.0335	–	0.0316
Importance sampling (Monte Carlo) with 1000 simulations	–	0.0325	–	0.0335	–	0.0324

Figure 3. Reliability Index and Probability of Failure for the Sliding Mode of Failure (Sujith et al. 2011)

The authors also developed design tables that provide the user with an appropriate factor of safety for a certain desired reliability index (Figure 4).

Coefficient of friction (μ)	Reliability index [COV(ϕ) = 10%]					
	β_{target} = 2.5			β_{target} = 3.0		
	$\phi = 20°$	$\phi = 30°$	$\phi = 40°$	$\phi = 20°$	$\phi = 30°$	$\phi = 40°$
0.4	1.86	1.84	1.97	1.89	2.07	2.21
0.5	1.85	1.85	2.07	1.91	2.12	2.25
0.6	1.85	1.85	2.20	1.94	2.13	2.31
	Reliability index [COV(ϕ) = 5%]					
	β_{target} = 2.5			β_{target} = 3.0		
	$\phi = 20°$	$\phi = 30°$	$\phi = 40°$	$\phi = 20°$	$\phi = 30°$	$\phi = 40°$
0.4	1.71	1.75	1.80	1.81	1.86	1.94
0.5	1.74	1.75	1.81	1.84	1.89	1.97
0.6	1.76	1.77	1.82	1.86	1.90	1.99

Figure 4. Recommended Factors of Safety for Sliding Failure (Sujith et al. 2011)

Zhang et al. (2013) analyzed two stability models for gravity retaining walls based on the upper-bound theory of limit analysis, where two failure modes were considered as a series of correlated systems. Monte Carlo simulations coded in MATLAB were used to calculate the reliability of the retaining wall. The authors considered a gravity retaining wall on a highway in Hunan Province-China as a case study.

The results indicated that analyzing a retaining wall using this method that applies Monte Carlo simulation and limit analysis theory is more accurate, safe and theoretically rigorous than the traditional approach. The authors observed that correlations between the multiple failure modes affected the reliability of the model, where higher reliability levels where obtained compared to the single failure mode.

8

Zhang et al. (2013) also studied the effect of different parameters on the design (internal friction angle, cohesion of backfill, friction coefficient soil-basement, and friction angle of backfill soil behind the retaining wall). They concluded that the cohesion of the backfill soil, the internal friction angle and the soil-wall friction coefficient have an impact on the reliability.

GuhaRay et al. (2014) considered four failure modes for retaining walls: base sliding, overturning, eccentricity (eccentricity > base width/6), and foundation bearing capacity failure. They highlighted the need for combining the sensitivity of the random variables with the probability of failure (Pf) of each failure mode to introduce a probabilistic risk factor (Rf).

The results showed that the eccentricity and the overturning modes of failure are governed by the friction angle of the backfill, while the bearing mode of failure is controlled by the friction angle and the cohesion of the foundation soil. Their study also concluded that the soil properties are positively correlated. The authors finally suggested modifications to the soil parameters and design of the structure according to the calculated Probabilistic Risk Factor.

Daryani and Mohamad (2014) used a reliability-based approach to analyze cantilever retaining walls embedded in granular soils using Monte Carlo Simulations (MCS) coded in MATLAB. The internal friction angle and void ratio of the soil were assumed to be correlated random variables, and the correlation lengths of soil parameters were assumed to be extremely large. They assumed that the system reliability is a series system, which is composed of the rotational and structural failure modes.

The results showed that the embedment depth ratio which is the ratio of the penetration depth (D) to the height of the wall (H) affects the rotational failure mode

(Figure 5) whereas the structural failure mode depends on the section modulus (Figure 6). Daryani and Mohamed (2014) concluded that an increase of D/H would result in an increase of the reliability index of the whole system. The section modulus of the wall can then be selected based on the depth (Figure 7). They also observed that the structural failure mode controls the limit state for a reliability index lower than 2.5 (Figure 8), whereas the rotational failure mode governs for cases with larger reliability indices.
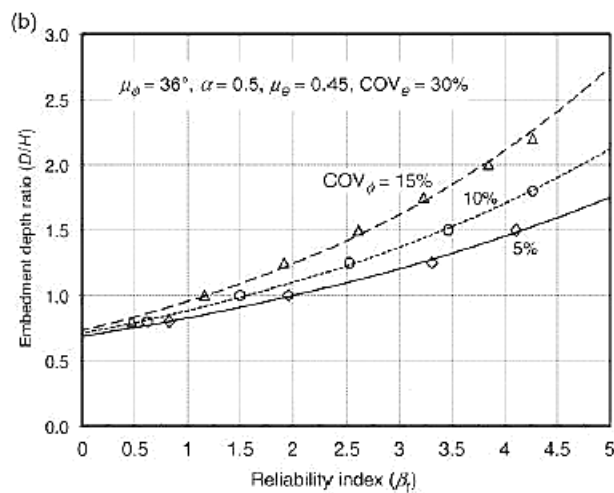
Figure 5. Effects of Variability in Soil Internal Friction Angle on Rotational Reliability Index (Daryani and Mohamad (2014))
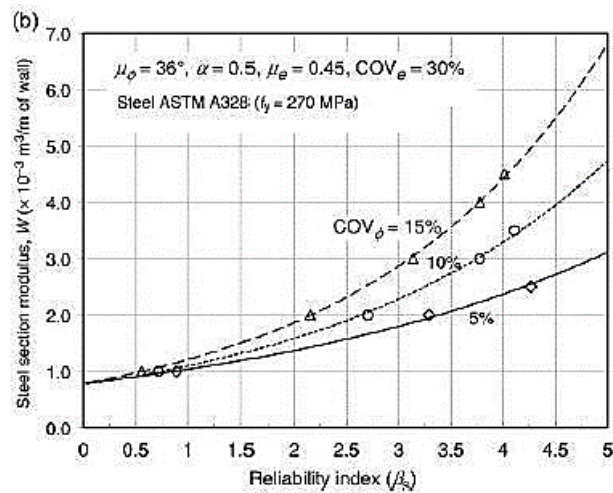
Figure 6. Effects of the Variability in Soil Internal Friction Angle on the Structural Reliability Index
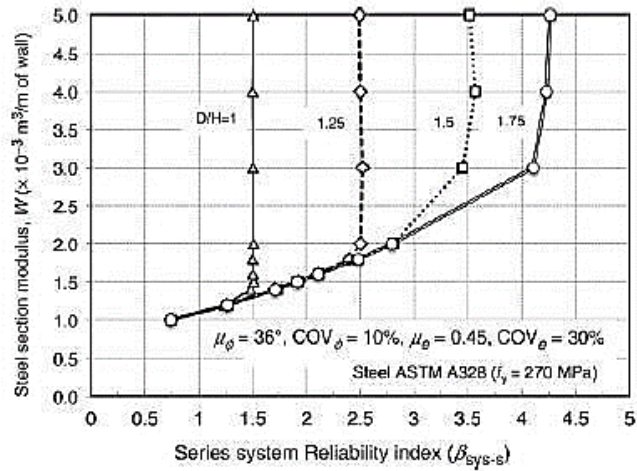
Figure 7. Variation of Series System Reliability Index (Bsys–S) With Section Modulus for Different Embedment Depth Ratio (D/H) (Daryani and Mohamad (2014))
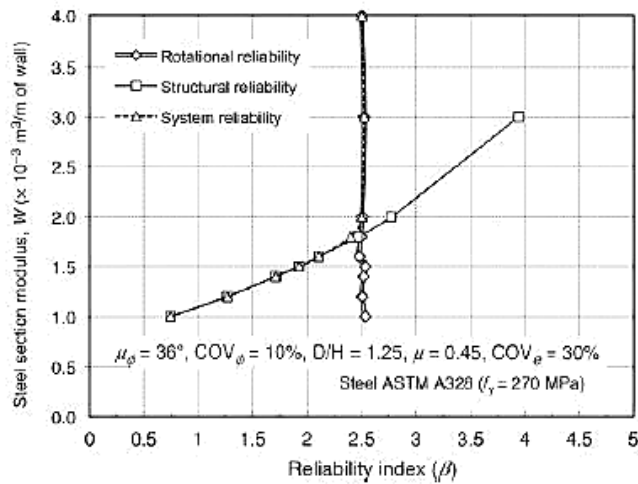
Figure 8. Variation of Component Reliability Indices Corresponding to Rotational and Structural Failure Modes and System Reliability Index (Bsys–S) (Daryani and Mohamad (2014))

2.2 Studies involving the design of retaining walls using FEM

Fenton et al. (2005) used non-linear finite element analysis in combination with random field simulation to find the effect of spatial variability on the active earth pressure on a retaining wall (Figure 9). They compared the active earth pressure resulting from this analysis with the one obtained by classical Rankine and Coulomb approaches. Furthermore, they investigated the effect of spatial variability on the global failure surface.

11

Fenton et al. (2005) found that the failure pattern is more complex than that obtained using the traditional theories, where the results show that the failure surface passes through the high friction angle region in the active case and that the location of the failure surface is controlled essentially by k_o (at-rest lateral earth pressure).
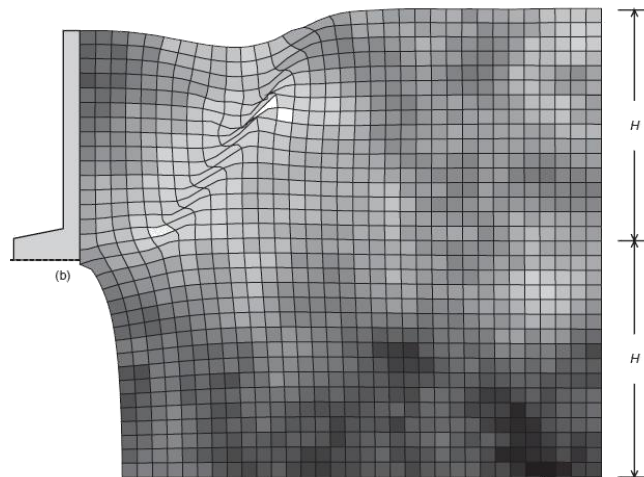
Figure 9. Active Earth Pressure Where the Soil Is Spatially Random (Fenton et al. (2005))

The authors estimated the probability that the driving force exceeds the resisting force to sliding for two cases: (1) correlated and (2) uncorrelated angle of friction $\emptyset$ and the unit of weight of soil. Results showed that a lower probability of failure was obtained when the friction angle and unit weight fields were correlated. In addition, the authors studied the effect of the coefficient of variation and the correlation between the angle of friction and the unit of weight on the resulting factor of safety. Fenton et al. (2005) concluded that the factor of safety is reduced when including a correlation between input parameters, and the influence of the friction angle is more important than that of the unit weight.

Griffiths et al. (2008) repeated the analysis done in 2005 but for the case of passive earth pressure (Figure 10). They showed that the failure occurs at regions of lower friction angles and doesn't follow the same path assumed in the traditional

theory. They also observed that the passive earth pressure in this case is 1.8 times lower than that obtained using Rankine's theory. Results also showed that more realistic random field could be obtained if samples are extracted from the soil near the wall.
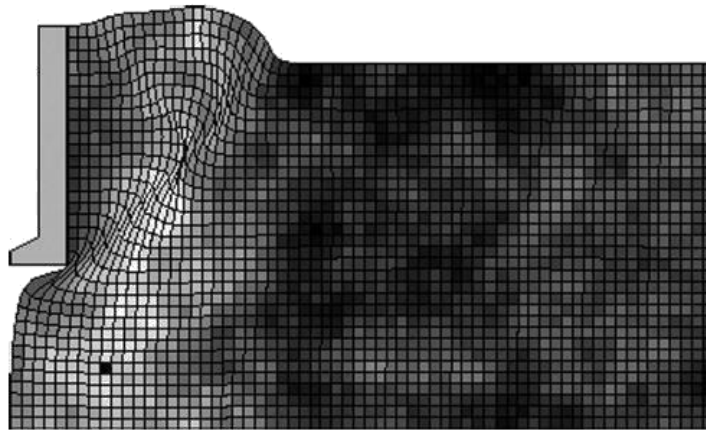
Figure 10. Passive Earth Pressure Where the Soil Is Spatially Random (Fenton et al. (2005))

Sayed et al. (2010) conducted a reliability analysis for a retaining wall using the first-order reliability method (FORM) and the finite element method using the finite element program

'GEOFEM'. The friction angle, unit weight, and wall-soil friction angle were considered as random variables. The analysis was applied to a case study. The results indicated that the probability of failure is high for the sliding mode of failure, whereas the wall is safe against overturning. The authors also proposed a procedure that can be used by designers to calculate the probability of excessive lateral displacement (Figure 11).
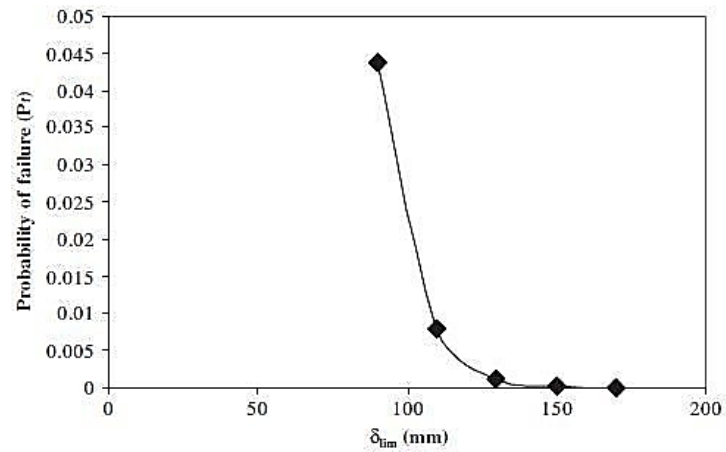
Figure 11. Probability of Exceeding the Limiting Lateral Wall Deflection for Reinforced Retaining Wall (Sayed et al. 2010)

Tang (2011) used the random finite element method (RFEM) to study the effect of uncertainty in the soil properties on excavation-induced deformations. To represent the geotechnical uncertainties, the author used joint probability distributions with random variables. Several finite element runs were also used to determine the probability of exceedance of maximum wall deflection. The author concluded that different levels of risk exist for the same wall deflection according to the degree of uncertainty specified (Figure 12).
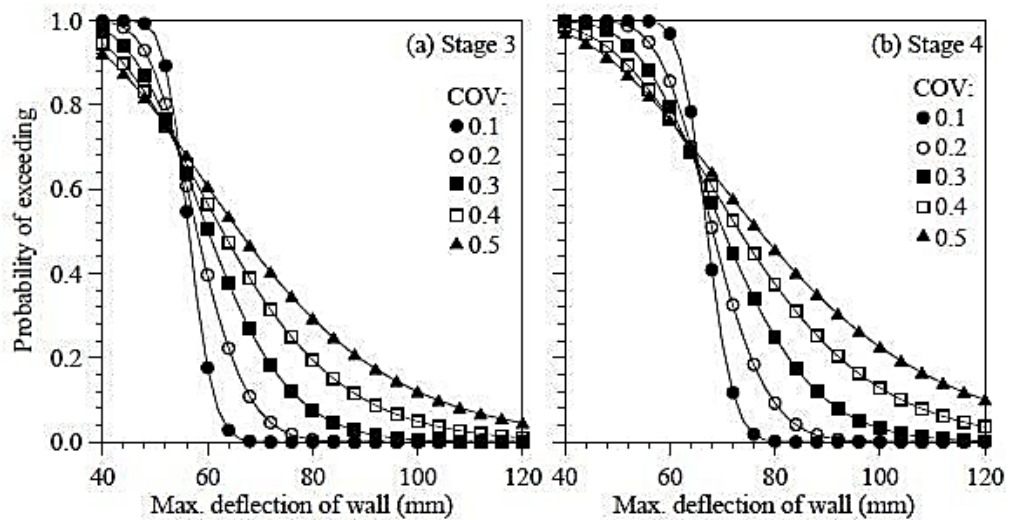
Figure 12. The Probability of Exceeding a given deflection with Respective to
Maximum Deflection of Retaining Wall (Tang (2011))

Dodagoudar et al. (2015) used the nonlinear finite element program GEOFEM
to analyze a reinforced concrete retaining wall to study the effect of the variability of
soil properties on the displacement of the wall (serviceability limit-state design). To
achieve this objective, the Young's modulus was considered as a random variable. The
results indicated that as the COV of the Young's modulus increases, the STD of
displacement increases, while the mean value is unaffected.

To validate the developed random finite element program, two examples were
considered: the first was obtained by Rahman and Rao (2001) and the second was from
Shinozuka and Yamazaki (1988). Dodagoudar et al. (2015) demonstrated that the
results obtained using GEOFEM agreed well with those reported in these earlier
studies.

Sert et al. (2016) used the random finite element method (RFEM) with Monte
Carlo Simulation (MCS) to study the effect of vertical spatial variability on the bending
moment and wall deflection of cantilever retaining walls, as well as the effect of the
number of Monte Carlo simulations on the predicted maximum lateral wall deflection

15

and maximum bending moment (Figure 13). The study was done at scales of fluctuation ranging from $\theta_v = 2m$ to $\theta_v = 100m$ and the internal friction angle was assumed to follow a lognormal distribution.

The results showed that the deterministic approach of analyzing the design of cantilever retaining walls overestimates the variation of wall deflection and bending moment and, depending on the selected limiting lateral wall deflection, the probability of failure may be thus either overestimated or underestimated. The authors concluded that a large number of MCS will result in a small variation in the calculated statistics of maximum lateral wall deflection, and that there is a strong positive correlation between maximum bending moment and the maximum lateral wall deflection (Figure 14).

Scale of fluctuation (θ)	Number of Monte Carlo simulation	Predicted STD of maximum lateral wall deflection (mm)	
		Mean	STD
2 m	100	12.20	0.87
	200	12.20	0.61
4 m	100	11.13	0.80
	200	12.40	0.62
10 m	100	18.58	1.33
	200	18.07	0.91
20 m	100	19.52	1.40
	200	19.98	1.01
50 m	100	22.64	1.62
	200	23.13	1.17
100 m	100	25.93	1.86
	200	24.61	1.24

Figure 13. Effect of Number of Simulations on Predicted Standard Deviation of Maximum Lateral Wall Deflection (COV=30%) (Sert et al. 2016)

(a) COV of = 10%   (b) COV = 30%
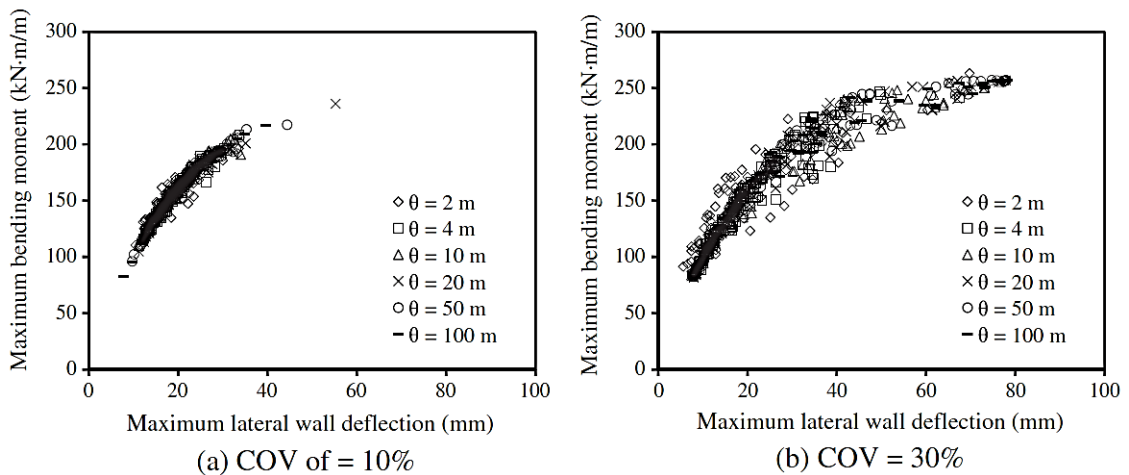
Figure 14. Correlation between Maximum Bending Moment and Maximum Lateral Wall Deflection at Various Levels of Spatial Variability (Sert et al. 2016)

The authors also showed that the mean values of the maximum bending moment and deflection increased with increasing scale of fluctuation, and that a small scale of fluctuation yields a small variation in the maximum lateral wall deflection and bending moment (Figure 16 and Figure 17).

(a) Mean of p_f (b) COV of p_f
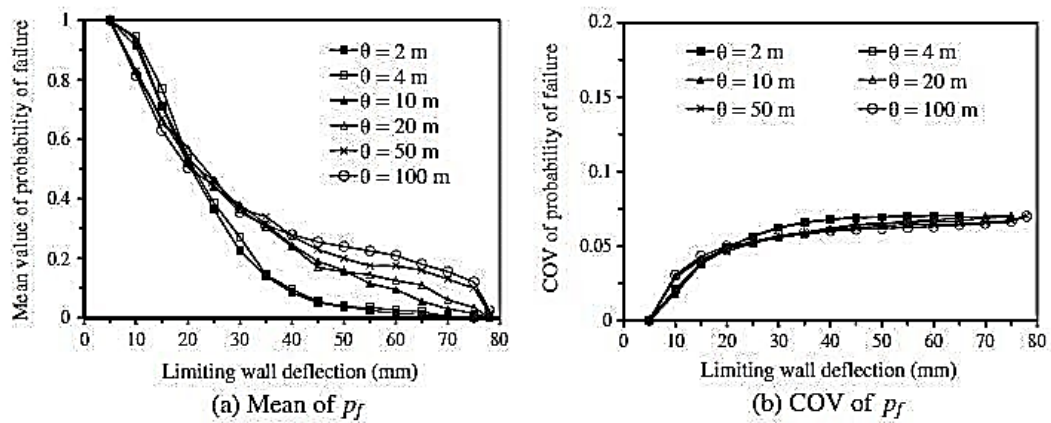
Figure 15. Effect of Spatial Variability on Probability of Exceeding the Specified Limiting Lateral Wall Deflection for Coefficients of Variation (COVs) Of Internal Friction Angle at 30 %.(Sert et al. 2016)

17
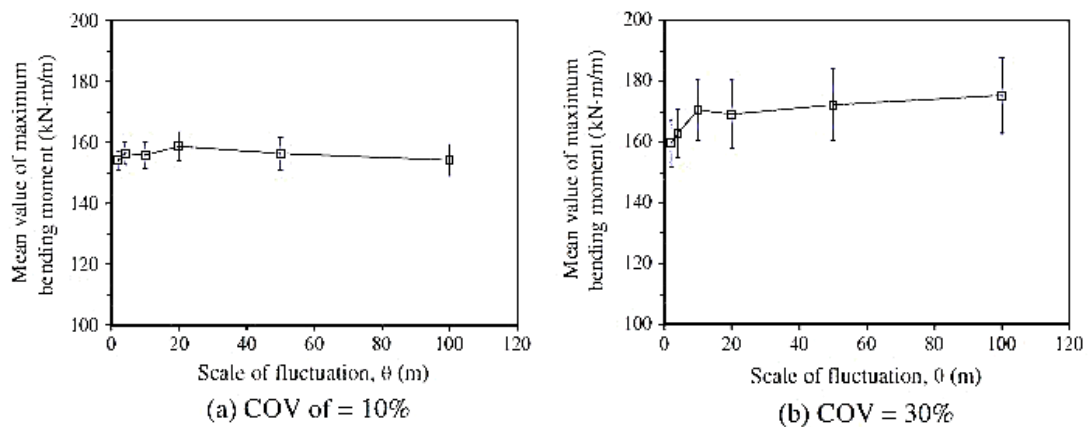
Figure 16. Effect of Spatial Variability on the Estimated Mean of Maximum Bending Moment (Sert et al. 2016)

Dasgupta et al. (2017) used the finite difference software FLAC® to study the effect of spatial variability on the failure surface and the lateral thrust of a 6m retaining wall. They applied Monte Carlo simulations to estimate the probability of failure using the covariance matrix decomposition technique. The authors assumed the friction angle as a random variable, while all parameters were taken as deterministic.

Dasgupta et al. (2017) deduced that deterministic procedures underestimate the lateral earth pressure when compared to the "true" lateral thrust (Figure 17), and that the thrust on the wall becomes higher when the variability of soil increases in the vertical direction. The worst case scenario was reached when the scale of fluctuation is high in both the vertical and horizontal directions (Figure 18).
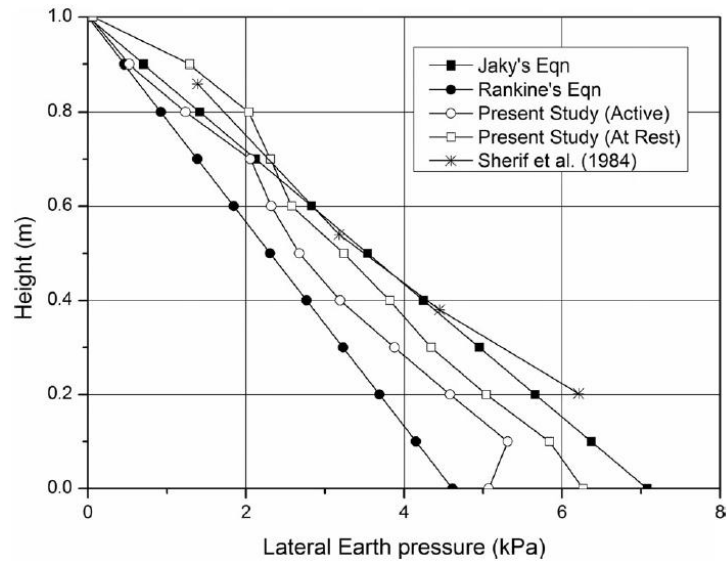
Figure 17. Validation of FLAC3D® Model Used in the Present Study. (Dasgupta Et Al. 2017)
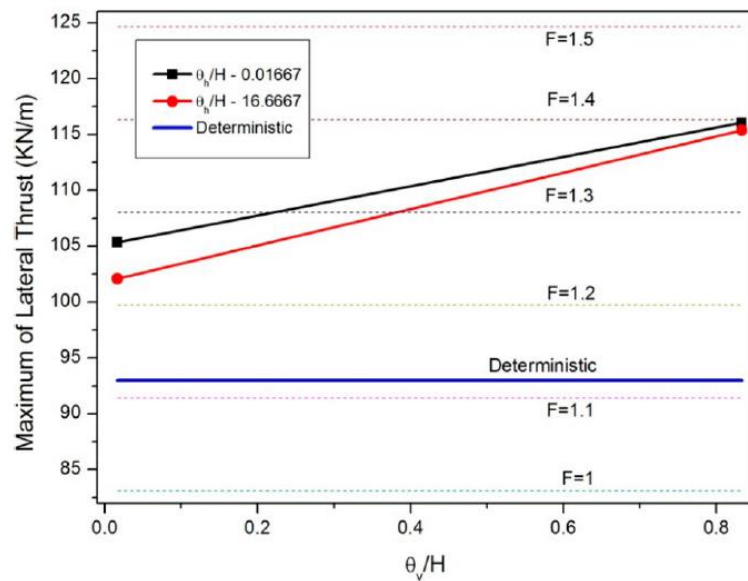
Figure 18. Variation of Maximum Lateral Thrust with Scale of Fluctuation (Dasgupta Et Al. 2017)

Results also showed that the inclination/angle of the failure wedge is not affected by the change in the spatial variability of the soil and that there is no correlation between the angle of failure and the determination of lateral thrust in the numerical analysis (Figure 19 and Figure 20).

Figure 19. Failure Surface Analysis – Homogeneous and Deterministic Soil (Dasgupta et al. 2017)
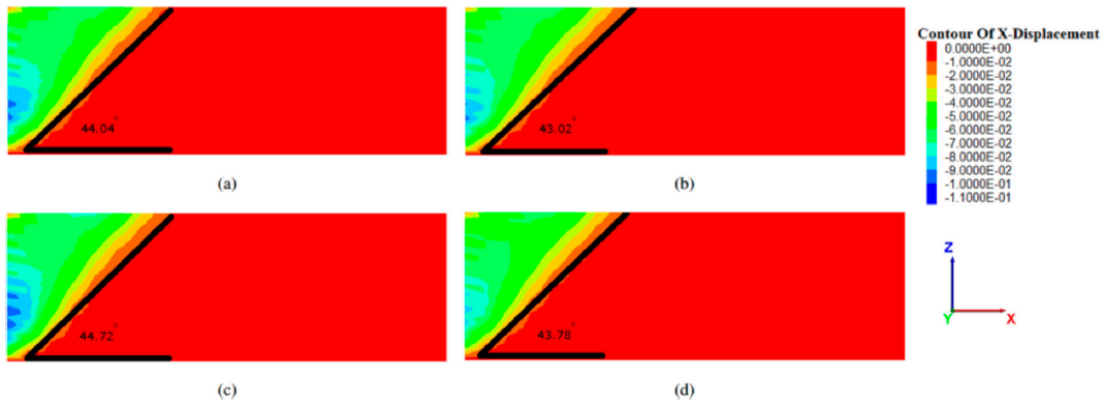
Figure 20. Failure Surface Analysis (A) Low θ_h, Low θ_v; (B) High θ_h, Low θ_v; (C) Low θ_h, High θ_v; (D) High θ_h, High θ_v(Dasgupta et al. 2017)

CHAPTER 3

DETERMINISTIC ANALYSIS

3.1 Wall dimensions and soil properties

A deterministic design of a selected wall is performed as a baseline case. The model consists of a 5m-wall that retains a cohesionless backfill, which lays on a layer of a stiff/dense foundation material. Figure 21 shows the section of the wall considered in the analysis, along with the corresponding dimensions.
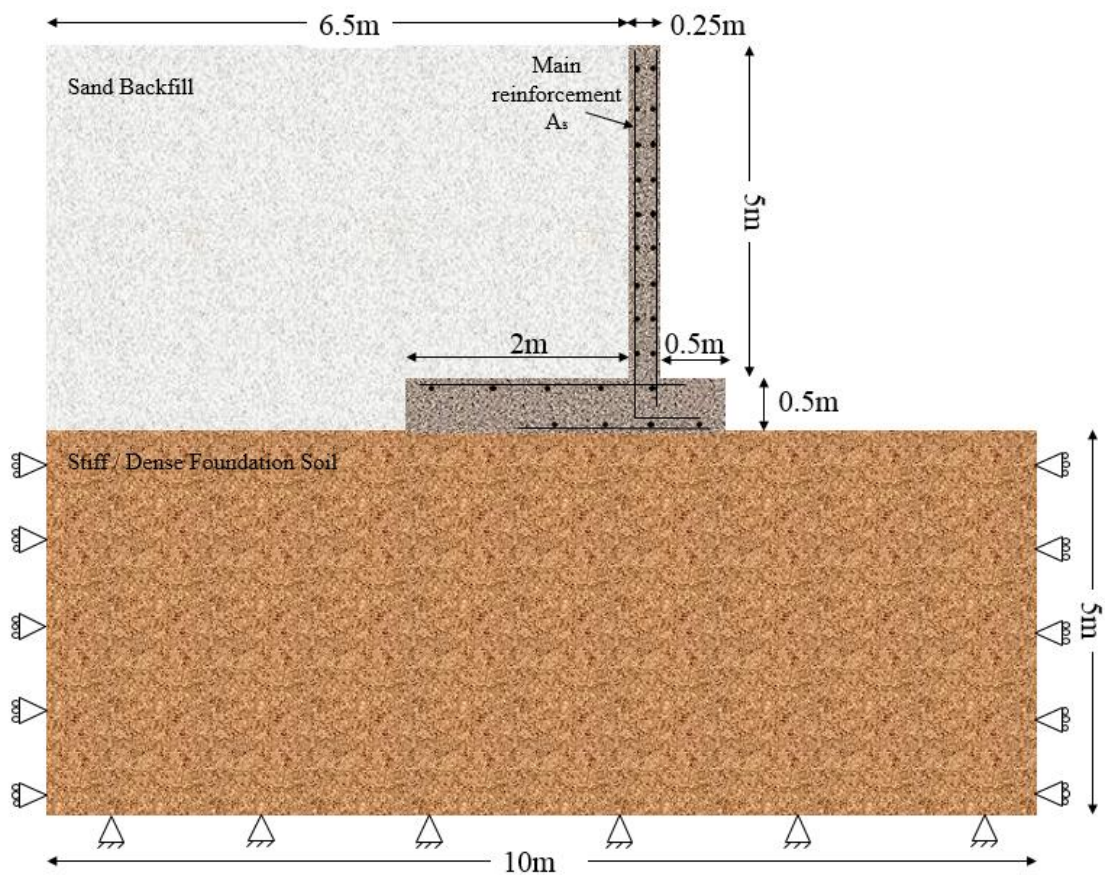
Figure 21. Wall Layout With Key Dimensions

The mechanical properties used in the deterministic analysis for the two soil layers are summarized in Table 1.

Table 1. Soil Parameters

Soil	Parameter	Notation	Value	Unit
Backfill soil layer	Friction angle	φ_1	33	°
	Unit weight	γ_1	18	kN/m³
	Cohesion	c_1	0	kPa
	Modulus of Elasticity	E_1	30	MPa
	Poisson's ratio	ν_1	0.3	-
	Dilation angle	Ψ_1	5	°
Foundation soil layer	Friction angle	φ_2	40	degree
	Unit weight	γ_2	19	kN/m³
	Cohesion	c_2	100	kPa
	Modulus of Elasticity	E_2	80	MPa
	Poisson's ratio	ν_2	0.25	-
	Dilation angle	Ψ_2	10	°

3.2 Failure Modes of Retaining Wall

The stability of the retaining wall is governed by three modes of failure:

1-Sliding Failure Mode: The wall should be designed such that the sum of the driving horizontal forces is less than the resisting forces.

2-Overturning Failure Mode: The sum of the moments about the toe that tend to overturn the wall should be less than the moment that stabilizes the wall, which is mainly the moment from the weights of the wall and the soil above the heel.

3-Bearing Failure Mode: The maximum applied pressure on the wall base q_{max} should be less than the ultimate bearing capacity of the foundation soil.

3.3 Design of the cantilever retaining wall according to Eurocode 7

Eurocode 7 proposed three approaches for the design of retaining walls. The difference between these approaches lies in the use of different partial factors for material properties, actions, effects of actions, and the resistance. Each country adopts a design approach according to its practice in geotechnical engineering. In this study,

design approach 1 which is applied in UK is selected. Based on this approach, two combinations should be checked, the first is called the "structural combination" where the partial factors are applied to the actions, and the second is called the "geotechnical combination" where partial factors are applied mainly to the geo-material properties. The design is governed by the more critical of the two. The partial factors recommended by Eurocode 7 are shown in Table 2.

Table 2. Partial Factors According to Eurocode 7.

Combination	Partial factors on actions			Partial factors on soil properties			
	$\gamma_{G,unfav}$	$\gamma_{G,fav}$	$\gamma_{Q,unfav}$	γ_φ	γ_c	γ_{cu}	γ_γ
1	1.35	1.0	1.5	1.0	1.0	1.0	1.0
2	1.0	1.0	1.3	1.25	1.25	1.4	1.0

$\gamma_{G,unfav}$: partial factor for unfavorable permanent action

$\gamma_{G,fav}$: partial factor for favorable permanent action

$\gamma_{Q,unfav}$: partial factor for unfavorable variable action

γ_φ: partial factor for the friction angle

γ_c: partial factor for the cohesion

γ_{cu}: partial factor for the undrained shear strength

γ_γ: partial factor for the weight density

Hence, to design a cantilever retaining wall according to Eurocode, the following steps are required:

STEP-1 Given the height of the wall, preliminary sizing of the different parts of the retaining wall (heel, toe, and stem) are assumed.

STEP-2 The dimensions of the wall are determined by checking its stability against

the three failure modes mentioned above, for the two combinations.

For the sliding failure mode, the ratio of the resisting forces to the driving

forces is:

$$\frac{cB + F_v \times \tan \delta}{F_h} \tag{1}$$

where c the cohesion of the foundation soil and B is is the width of the footing.

The value of c is divided by the partial factor proposed by Eurocode $\gamma_c = 1.0$ in

combination 1 and by $\gamma_c = 1.25$ in combination 2 (Table 2). F_v is the sum of the vertical

forces which constitute a favorable action that stabilizes the wall. δ is the soil-structure

interface friction angle (assumed to be equal to 2/3 of the friction angle of the

foundation soil). The value of $\tan \varphi$ is divided by the partial factor proposed by

Eurocode $\gamma_\varphi = 1.0$ in combination 1 and $\gamma_\varphi = 1.25$ in combination 2 (Table 2). F_h is the

sum of horizontal forces due to earth pressure.

$$F_h = k_a \times \gamma_1 \times \frac{H^2}{2} \tag{2}$$

The value of the active earth pressure k_a is calculated using Coulomb equation:

$$k_a = \frac{cos^2(\varphi - \alpha)}{cos^2\alpha \times cos(\alpha + \delta) \times (1 + \sqrt{\frac{sin(\varphi + \delta) \times sin(\varphi - \beta)}{cos(\delta + \alpha) \times cos(\alpha - \beta)}})^2} \tag{3}$$

Where φ: angle of friction, δ: angle of friction between structure and soil, β:

slope inclination, and

α: back face inclination of the structure. The value of F_h (unfavorable

permanent actions that destabilize the wall) is multiplied by 1.35 in combination 1 and

by 1.0 in combination 2 (Table 2).

For the overturning failure mode, the ratio of the resisting moment to the overturning moment is M_v / M_h, where M_v is the sum of the moments resulting from vertical loads, which stabilize the wall and M_h is the sum of the moments resulting from horizontal loads that tend to overturn the wall. The unfavorable permanent actions are also multiplied by 1.35 in combination 1 (Table 2).

For bearing capacity, the ratio of the ultimate bearing capacity of the soil to the maximum bearing pressure on the footing is given by q_u / q_{max}.

$$q_u = c N_c S_c d_c i_c + \gamma D N_q S_q d_q i_q + + 0.5\gamma B' N_\gamma S_\gamma d_\gamma i_\gamma \qquad (4)$$

N_c, N_q, N_γ : bearing capacity factors.

S_c, S_q, S_γ : shape factors.

d_c, d_q, d_γ: depth factors.

i_c, i_q, i_γ : inclination factors.

q_{max} is equal to $\frac{Q}{Bb}(1 + \frac{6 \times e}{B})$ for $e < \frac{B}{6}$ and $\frac{4Q}{3b(B-2e)}$ for $e > \frac{B}{6}$

Where: e is the eccentricity, Q is total vertical load, B is base width, b is base length=1m.

The values of c and $\tan \varphi$ are divided by the partial factors given in Table 2 for combination 2.

STEP-3 For the wall dimensions shown in Figure 21 and the soil properties presented in Table 1, the calculations for the three geotechnical failure modes are presented in are summarized in Table 3

Table 3. Failure Mode for The Two Combinations

Failure modes	Combination 1	Combination 2
Sliding: $(cB + F_v \times \tan \delta) / F_h$	2.26	2.68
Overturning: M_v / M_h	1.15	1.25
Bearing capacity. q_u / q_{max}	5.21	5.13

STEP-4 For the structural failure modes, the magnitude of the bending moment and

shear force are calculated and multiplied by 1.35 in combination 1 (Table 2).

The critical values are considered in the design. The calculations are

summarized in Table 4.

Table 4. Values of shear and moment for the two combinations

Outputs	Combination 1	Combination 2
Bending moment (kN.m)	133.8	123.7
Shear force (kN)	80.3	73.8

The required steel area is calculated using the equations proposed by Eurocode

7.

$$A_s = \frac{M}{0.87 \times f_y \times Z} \tag{5}$$

Where

$$Z = d \times \left(0.5 + \sqrt{0.25 - \frac{k_m}{1.134}} \right) \tag{6}$$

$$k_m = \frac{M}{(b \times d^2 \times f_{ck})} \tag{7}$$

f_y is the yield strength of steel assumed to be equal to 420 MPa, f_{ck} is the

compressive strength of concrete at 28 days assumed to be 25 MPa, d is the effective

depth, and M is the bending moment. The value of the unfavorable permanent actions is

multiplied by 1.35 in the combination 1.

The calculations of the required steel area and number of bars are summarized

in the Table 5:

Table 5. Calculations of The Number of Steel Bar / m

Bending moment (KN.m)	133.8
$d\ [mm]$	205
$k_m = \dfrac{M}{(b \times d^2 \times f_{ck})}$	0.1274
$Z = d \times \left(0.5 + \sqrt{0.25 - \dfrac{k_m}{1.134}} \right)$	0.17
$A_s = \dfrac{M}{0.87 \times f_y \times Z} \left[\dfrac{mm^2}{m} \right]$	2155
Number of bar/ m	7 bars/m (diameter 20 mm)

The area of steel should be greater than the minimum required area of tension

steel $A_{s\ min}$ proposed by Eurocode 2: $A_{s\ min} = 0.26 \times \left(\dfrac{f_{ctm}}{f_y} \right) \times b \times d$ where f_{ctm} is the

mean value of axial tensile strength.

$A_{s\ min} = 330$ mm2/m $< A_s$

The resisting shear force of the wall is:

$$V_{res} = 0.12 \times K_v \times b \times d \times (100 \times f_{ck} \times \rho)^{\frac{1}{3}} \qquad (8)$$

Where $k_v = 1 + \sqrt{\dfrac{200}{d}}$ and $\rho = \dfrac{A_s}{b \times d}$

$V_{res} = 145$ kN $>$ calculated shear force.

CHAPTER 4

PROBABILISTIC ANALYSIS

4.1   Introduction

The design wall that is depicted in Figure 21 and subject of the deterministic analysis of the previous section, was analyzed probabilistically in FLAC 2D® by assuming that the friction angles of the backfill and foundation soil are modeled using random fields. In order to isolate the impact of the friction angle on the response, all other soil parameters in Table 1 were assumed to be deterministic.

The main objective of the probabilistic study is to investigate the effect of statistical parameters of the random field of the friction angle ($\mu_\varphi, COV_\varphi, \theta_\varphi$) on the structural response of the retaining wall. To achieve this objective, the analysis was conducted for different mean, correlation length, and COV of friction angle. The assumed values for these parameters are shown in Table 6 and are expected to cover the practical/realistic range of possible values for each parameter.

Table 6. Statistical Parameters of The Friction Angle φ

Parameter	Values
Mean (degrees)	30, 33, 36
COV (tan φ)	0.05, 0.1, 0.15, 0.2
Vertical and horizontal correlation length (m)	1, 2.5, 5, 10, 25

4.2   Numerical modelling

FLAC® (from Itasca) is a robust software package for modeling soil and soil-structure interaction problems. The software-specific FISH language allows faster model construction, generation of random fields, and the automation of simulations. The

software was utilized to build a wall-soil model (Figure 22) that has the same

dimensions as the model used in the deterministic analyses (Figure 21). Plane strain 2D

conditions were adopted with the Mohr-Coulomb constitutive model for both the

backfill and the foundation soil layers. Due to limitations in computational efforts, and

in order to account for the developed failure wedge, the backfill soil layer width was set

to extend up to 6.5m from the wall and the depth of the foundation soil was taken to be

5m. The boundary conditions were fixed at the bottom and laterally restrained at the

sides of the model. Square elements were chosen with a side of 1/6m to represent the

soil body. A code was developed to generate random fields for the friction angle of the

soil using R software as presented in the appendix. The model size, boundary conditions

and mesh size were checked to have little/no impact on the calculated wall response.
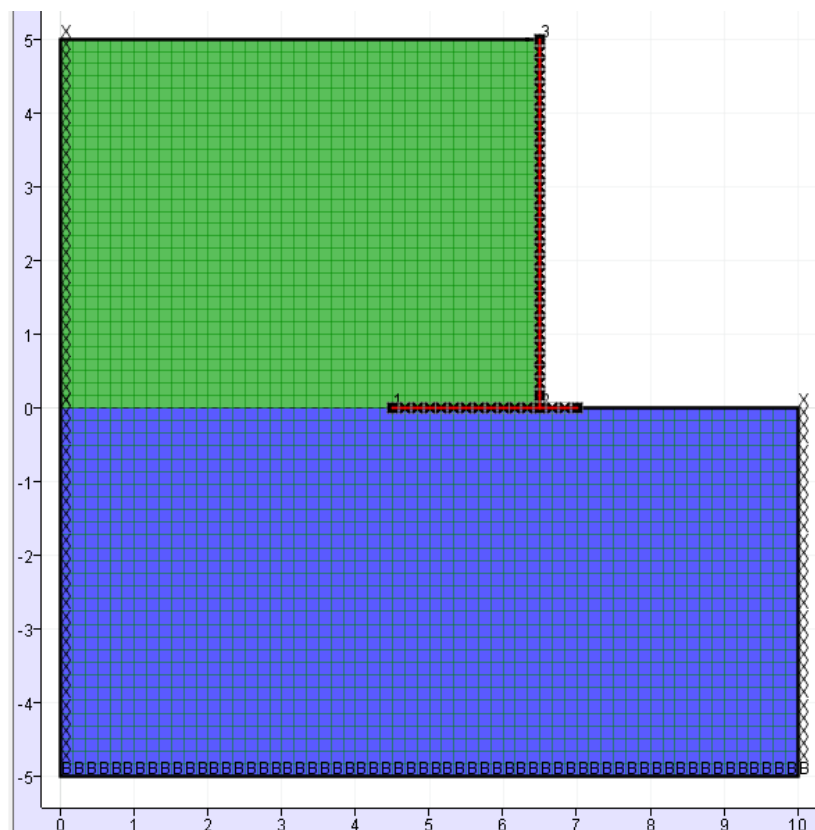
Figure 22. FLAC® Model: Soil Layers and Dimensions

The probabilistic study was conducted using Monte Carlo Simulations. The

main output parameters of interest are the displacement of the wall, the bending moment

at the wall base, the maximum shear at the base of the wall, and the resultant lateral

thrust on the wall. Based on trial and error analyses, a decision was made to conduct the

probabilistic analysis using 1600 random field simulations. This number of realizations

was found adequate to yield 95% confidence in the calculated mean values for all output

parameters within 1% error. The required number of simulations was calculated using

the following formula:

$$N = \left(\frac{196}{\% \; Error \; in \; \mu_Y}\right)^2 COV_Y{}^2 \tag{9}$$

Where COV_Y is the coefficient of variation of the output "Y" and "% Error

in μ_Y" is the degree of precision of the mean of "Y". As an example, the required

number of realizations for a percentage error in $\mu_{x-displacement}$ that equals 1% and

a $COV_{x-displacement}$ of 0.14 (highest COV observed in this study) is 750 realizations.

1600 realizations were adopted in this study.

The interface soil-structure between the wall and the backfill behavior is

governed by the normal stiffness (k_n) and shear stiffness (k_s). It is recommended that k_n

and k_s be set to ten times the equivalent stiffness of the stiffest neighboring zone (Itasca

Consulting Group, 2011):

$$k_n = k_s = 10 \; max \frac{k + \left(\frac{4}{3}\right) G}{\Delta z_{min}} \tag{10}$$

Where: k & G are the bulk and shear moduli, respectively. k & G are

calculated by the following equations: $k = \frac{E}{3 \times (1 - 2 \times v)}$ and $G = \frac{E}{2 \times (1 + v)}$

The values of E and v are presented in Table 1.

Δz_{min} is the smallest width of an adjoining zone in the normal direction and it

equals to 0.1m (mesh resolution adjacent to the interface zone). Using the previous

equations, k_s and k_n of the interface wall-soil are assumed to be equal to 9.6 MPa/m for

the foundation layer, and 4.04 MPa/m for the backfill layer.

The random field of the friction angle is defined by three parameters: the mean

of the variable, the coefficient of variation, and the correlation length. The correlation

structure for an anisotropic random field is computed using equation 11:

$$\rho(\Delta x, \Delta z) = \exp\left(-\frac{2|\Delta x|}{\theta_h} - \frac{2|\Delta y|}{\theta_v}\right) \tag{11}$$

Where Δx and Δy are the horizontal and vertical distances between two points

and θ_h and θ_v are the horizontal and vertical correlation lengths.

Two cases of spatial variability of soil properties are analyzed: (1) Isotropic

spatial variability, where the horizontal correlation length θ_h is equal to the vertical

correlation length θ_v and (2) Anisotropic spatial variability where the horizontal

correlation length is different than the vertical correlation length. The second case is

more realistic since soils in nature are formed/exist in roughly horizontal layers.

Figure 23 shows the spatial variability of the friction angle for four isotropic

random fields, with correlation lengths ranging from 1.0m to 25.0m. Figure 24 is a

similar plot but generated for anisotropic random fields, with a constant horizontal

correlation length of 10m and a varying vertical correlation length. The generation of

the random field for the friction angle is performed using the statistical software **R** and

then exported to FLAC® by the following procedure: Using the FISH function that is

built-in FLAC®, the coordinates of each element of soil geometry are exported to the

software **R** to calculate the distance between any two elements. The correlation matrix

which designates the correlation coefficient between any two elements in the finite

difference mesh is constructed based on the Markovian correlation function in equation

11. Monte Carlo Simulations using a lognormal distribution for the friction angle are then generated from the mean vector and covariance matric of the different soil elements. The simulated values of φ for each random field realization are obtained and stored in separate text files. Several functions in the FLAC® software are called-in to draw the geometry of the model, map the friction angle corresponding to each element, and run the model to obtain the different required outputs.
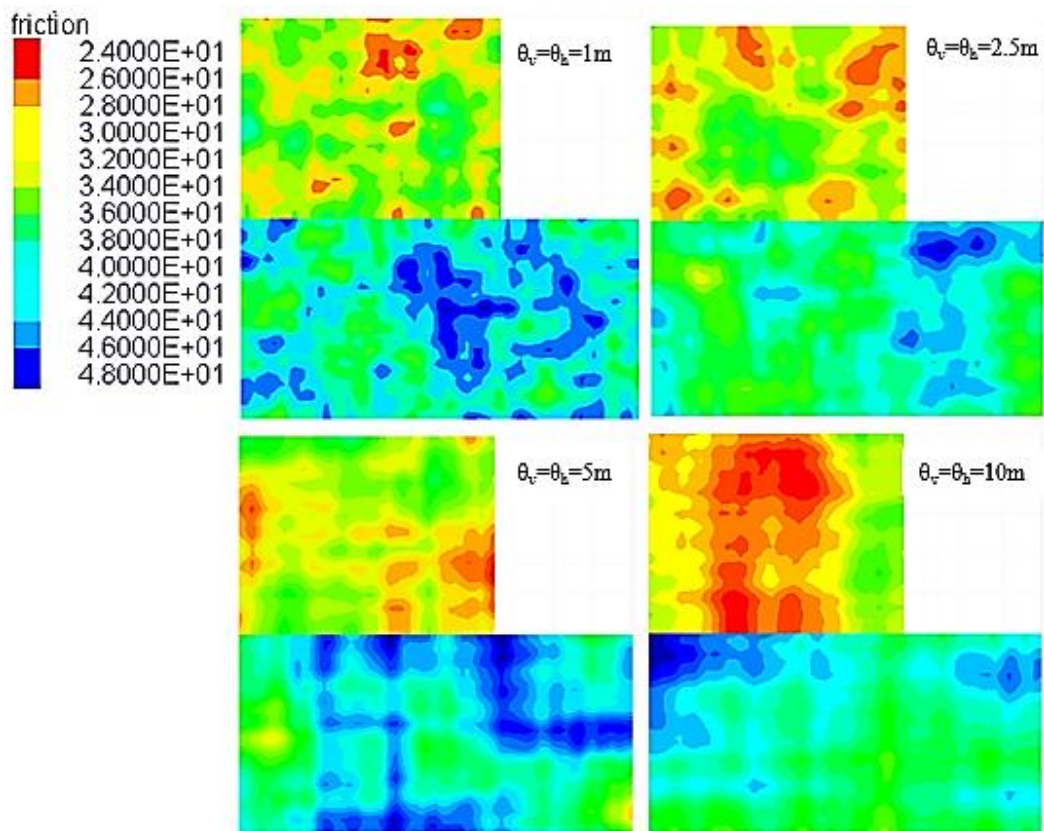
Figure 23. Spatial Variability of The Friction Angle for Different Correlation Lengths (Isotropic Case)
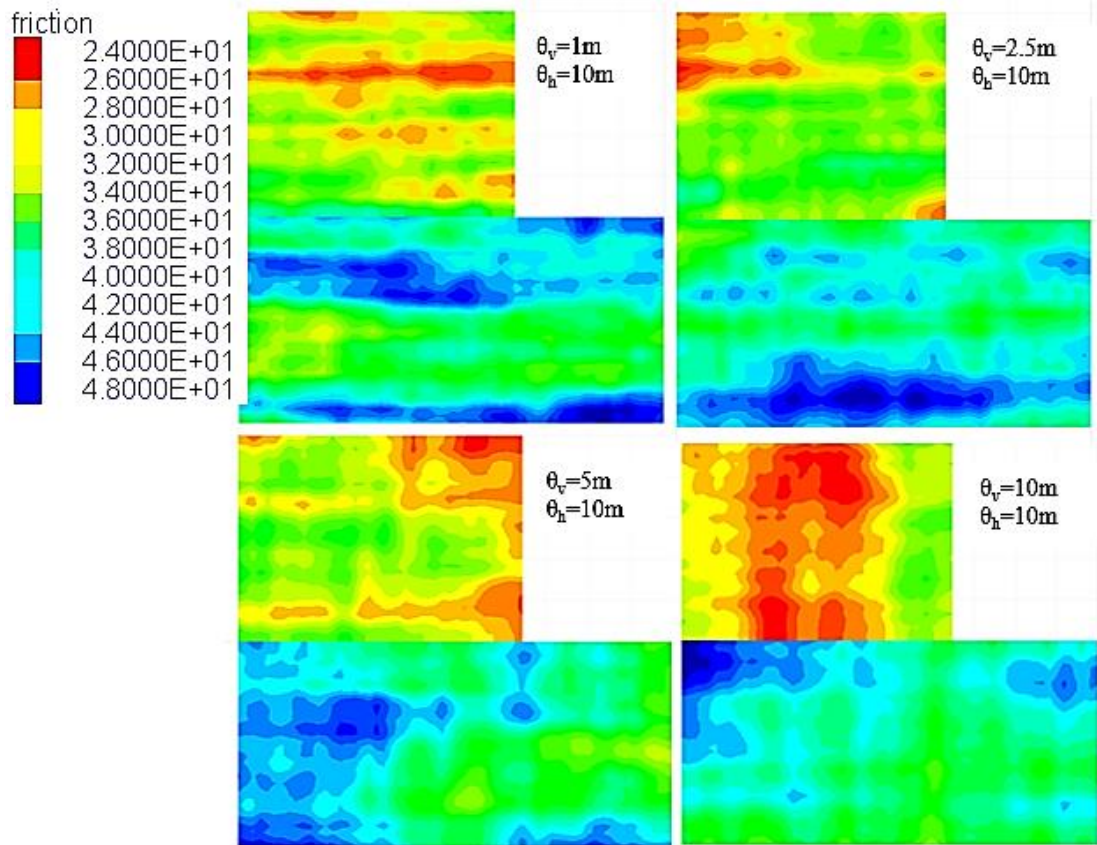
Figure 24. Spatial Variability of The Friction Angle for Different Correlation Lengths (Anisotropic Case)

CHAPTER 5

RESULTS OF THE NUMERICAL ANALYSES

5.1 Introduction

The outputs of interest of the Monte Carlo Simulations (Maximum moment, maximum shear, lateral earth pressure, and maximum horizontal displacement) are presented graphically in Figure 25. The means, standard deviations STD, and coefficient of variation COVs for these outputs are shown for all the cases analyzed in the first section of this part. In the second section, the resulting probabilities of failure based on the EUROCODE 7 recommended partial factor are displayed. In the final section, partial factors that result in a targeted reliability index are proposed.
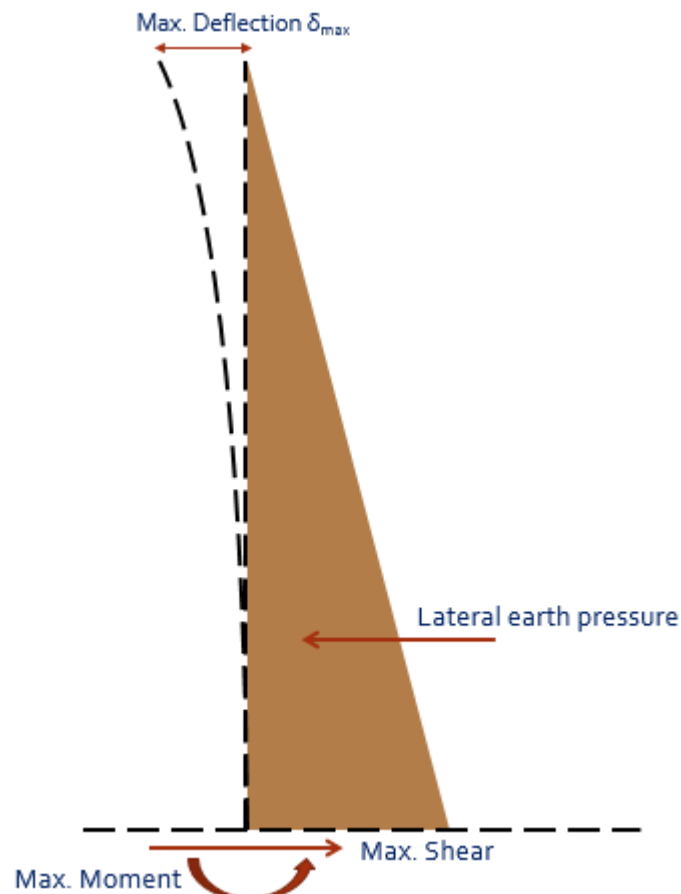
Figure 25. The Outputs of the Monte Carlo Simulations

5.2   Isotropic correlation case

5.2.1   *Base case scenario (deterministic foundation layer)*

Figure 26 shows the variation of the mean, STD, and COV of the maximum bending moment and maximum shear force with the correlation length for the base case scenario, in which $\mu(\varphi) = 33^\circ$ and a COV $(\tan \varphi) = 0.1$ are adopted. In the base case scenario, the friction angle of the foundation soil is assumed to be deterministic. It is observed that the mean of the maximum moment equals 104 kN.m and it is not affected by the change in correlation length of friction angle. This mean value is slightly higher than the deterministic value of the maximum moment (99 kN.m) obtained in FLAC® using a deterministic friction angle of 33 degrees. The STD of the moment increases asymptotically from 3.7 to 10kN.m as the correlation length increases from 1 to 10. For correlation lengths that are greater than 10, the value of STD remains approximately constant. This is due to the fact that the correlation length becomes larger than the height of the wall. The corresponding coefficients of variation of the maximum moment increase from 0.035 to 0.1 as the correlation length increases from 1m to 25m. Similar trends are observed for the maximum shear force with a probabilistic mean value that is identical to the deterministic value of 59.5kN and a standard deviation that increases from 1.6 to 4.3kN, resulting in COVs that range from 0.026 to 0.07 for the maximum shear.

The increase in the COVs of the maximum moment and shear with the correlation length is expected. As the correlation length of the friction angle increases, the random field of the friction angle becomes more and more spatially correlated and homogeneous. This reduces the positive impact of variance reduction due to averaging

of the friction angle in the failure zone behind the wall on the overall uncertainty in the output parameters (moments and shears). For smaller correlation distances, the random field in any given simulation is more erratic, resulting in variance reduction in the average friction angle in the soil elements in the failure zone behind the wall. This will reduce the uncertainty in the maximum moments and shears as evidences in the smaller COVs at small correlation lengths.
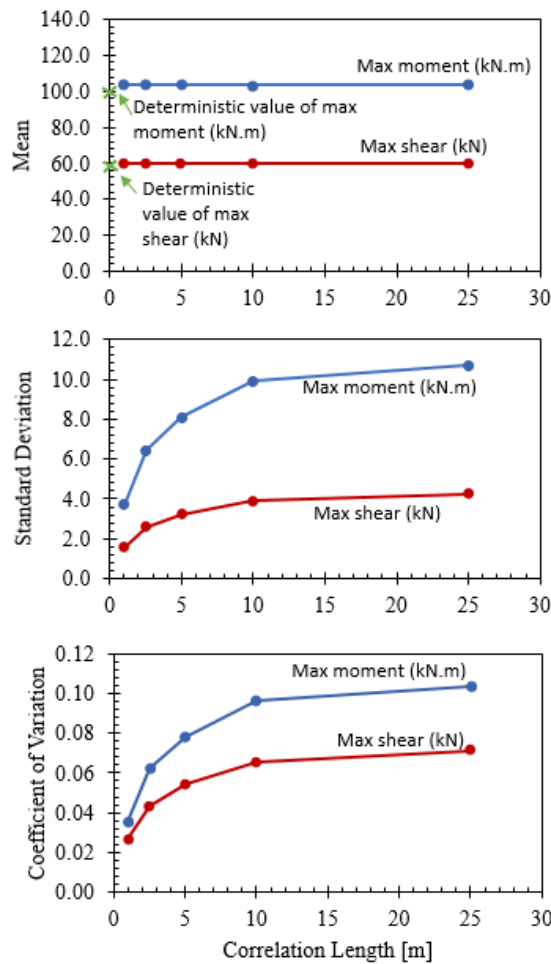
Figure 26. The Variation of The Mean, STD, and COV of The Maximum Bending Moment and Shear Force With The Correlation Length (μ (φ) = 33°, cov (tan φ) =0.1)

Figure 27 shows the variation of the mean, STD, and COV of the maximum horizontal displacement and the resultant earth pressure with the correlation length for the base case scenario with a $\mu(\varphi)$ = 33° and a COV (tan φ) =0.1. The mean of the

maximum displacement remains constant and equal to 21.6mm as compared to the

deterministic value (21.3mm). The STD increases from 1mm to around 3mm when the

correlation length increases from 1m to 25m. The coefficient of variation increases from

4.4% to 13.3% for a correlation length of 25m.

On the other hand, the mean of the resultant lateral force is constant and equal

to the value of the shear force (~60kN). This value is similar to the value obtained from

the deterministic approach (59.5kN). The STD increases from 1.8kN to 4.6kN as the

correlation length increases from 1 to 25m. The COV also increases from 0.036 for $\theta_h=$

$\theta_v=1$m to 0.093 for $\theta_h=\theta_v=25$m.

The variation of the COVs of the four outputs (maximum bending moment,

maximum shear force, maximum horizontal displacement, and resultant lateral force)

with the correlation length in consistent with the concept of the averaging effect of soil

properties along the correlation zone. Thus, as the scales of fluctuation decrease with

respect to the scale of the failing wedge, the COVs of the outputs decrease. On the other

hand, when the scales of fluctuation approach the dimensions of the soil wedge, the

COVs of the outputs reach asymptotic values.
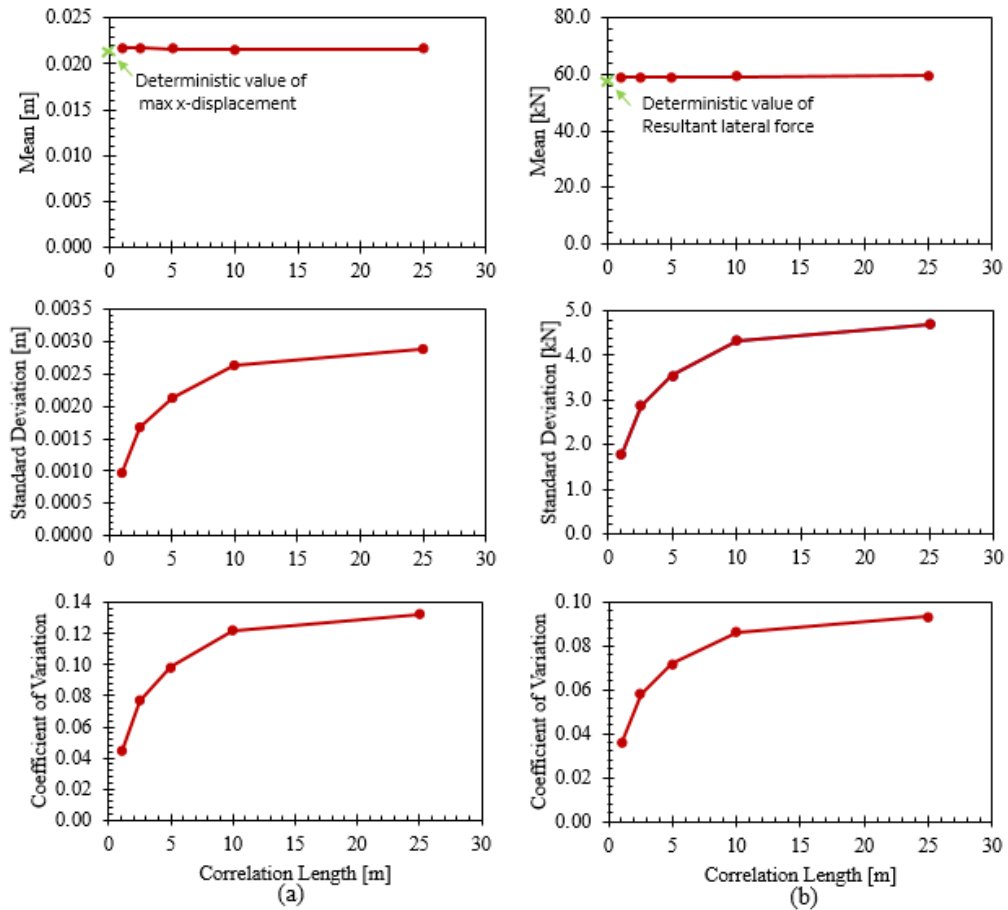
Figure 27. The Variation of The Mean, STD, and COV of (A) The Maximum Horizontal Displacement(M), and (B) The Resultant Lateral Force(Kn) With The Correlation Length(μ (φ) = 33º, cov (tan φ) =0.1)

5.2.2 *Effect of spatial variability in backfill friction angle*

The results in Figures 25 and 26 pertain to the case with a friction angle with a COV of 0.1. Figure 28 shows the variation of the COVs of the four output parameters with the COV of the friction angle for the case with $\theta_h = \theta_v = 1$m. The COV of the maximum moment, maximum shear, maximum displacement, and resultant earth pressure increase linearly when the COV of the friction angle increases from 0.05 to 0.2. The maximum value is 0.08 for the maximum x-displacement which corresponding to a COV (tan φ) equal to 0.2. The relatively small COVs of the outputs as compared to the COV (tan φ) are attributed to variance reduction due to averaging, for the case with the

38

small correlation length (1m) of the friction angle.
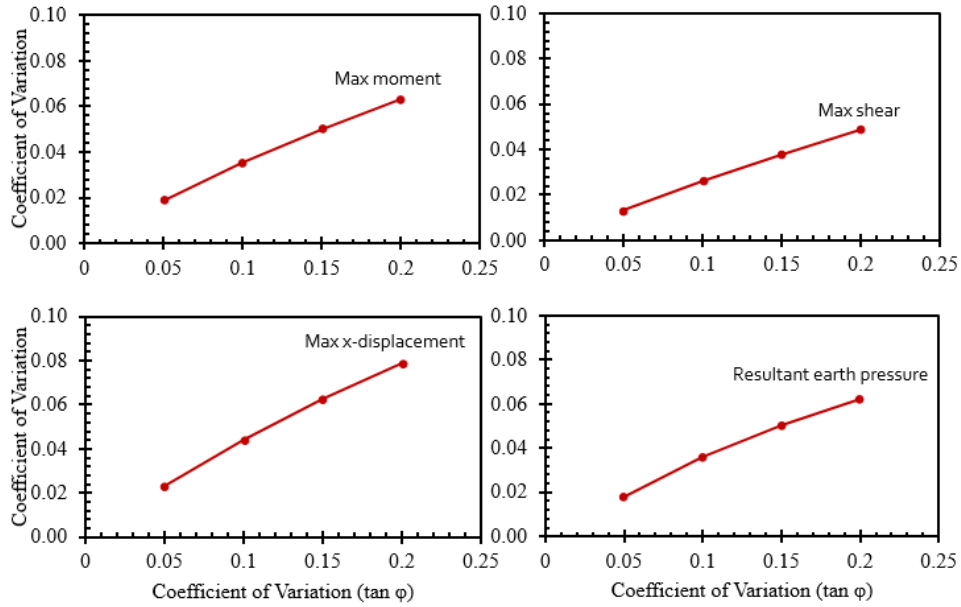
Figure 28. The Variation of COV of The Four Outputs for Different COV (tan φ)(μ (φ) = 33°, $\theta_h = \theta_v = 1m$)

5.2.3 *Effect of spatially variable foundation soil*

In an effort to explore the effect of spatial variability of the foundation soil layer on the structural behavior of the cantilever retaining wall, the analyses are repeated by considering a soil under the footing with a random friction angle having a mean (φ) of 40°. The simulations are conducted for different correlation lengths and different COVs of the friction angle.

Figure 29 shows the variation of the COV of the four outputs for different correlation lengths for two cases: 1 variable layer (only the backfill soil is considered as random soil) and 2 variable layers (the backfill and the foundation soils are considered as random soil) for the isotropic case (μ (φ) = 33°, COV (tan φ) =0.1). It is noticeable from all the cases that the variability in the foundation layer has practically no effect on the structural demands and deflections of the retaining wall. These results may be

explained by the fact that the bending moment, shear force, and resultant earth pressure are not sensitive to changes in the foundation soil friction angle, particularly given that the soil has a relatively high cohesion value that was kept as a constant (100 kPa) in the analysis. In this case, the structural demands on the wall are more affected by the friction angle in the backfill soil. The same conclusions were obtained for the cases with anisotropic soil properties.
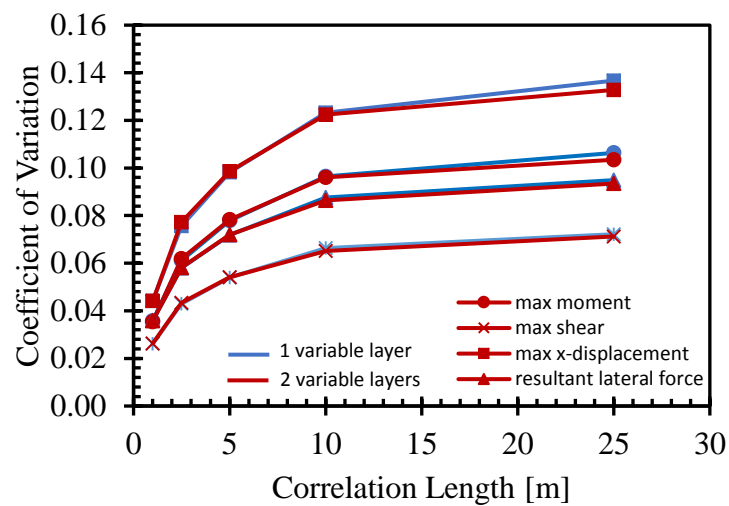
Figure 29. The variation of COV of the four outputs for different correlation lengths for two cases: 1 variable layer and 2 variable layers (isotropic case, μ (φ) = 33°, COV (tan φ) =0.1)

5.3 Case of anisotropic random field for φ

In an effort to investigate the impact of the correlation structure of the random field of the friction angle on the results, simulations were conducted for two cases: The first is the isotropic spatial variability considering similar correlation lengths in the vertical and horizontal directions ($\theta h = \theta v$), and the second is the anisotropic spatial variability, where the horizontal correlation length is fixed at a constant value of 10 m and the vertical correlation length is varied. Simulations were conducted for five vertical correlation lengths of 1, 2.5, 5, 10 and 25m. The variation of the statistical parameters

40

(mean, STD, and COV) of the output variables are plotted as a function of the vertical

correlation length for these two cases for comparison.

5.3.1 *Comparison between isotropic and anisotropic fields.*

The variation of the COVs of maximum moment, maximum shear, maximum

x-displacement and lateral earth pressure with the vertical correlation length for the base

case with ($\mu(\varphi) = 33^\circ$, COV (tan φ) = 0.1) are shown in Figure 29. For the anisotropic

case, the horizontal correlation length is fixed at 10m.

It can be noted from Figure 30 that the COVs of the different outputs have the

same trend when comparing the isotropic and anisotropic cases. For vertical correlation

lengths less than 10m, the COVs of the four outputs for the anisotropic case are greater

than those of the isotropic one. At a vertical correlation length that is equal to 10m, the

two curves overlap. Finally, for vertical correlation lengths that are greater than 10m,

the COVs of the four outputs for the isotropic case are greater than those of the

anisotropic case. For the first region ($\theta_v < 10$m), the averaging effect applies in both

directions (horizontal and vertical) for the isotropic case, while for $\theta_v > 10$m, less

averaging effect takes place in the isotropic case with $\theta_v = \theta_h = 25$m because of the

larger correlation lengths as compared to the anisotropic case ($\theta_v = 25$m, $\theta_h = 10$m).
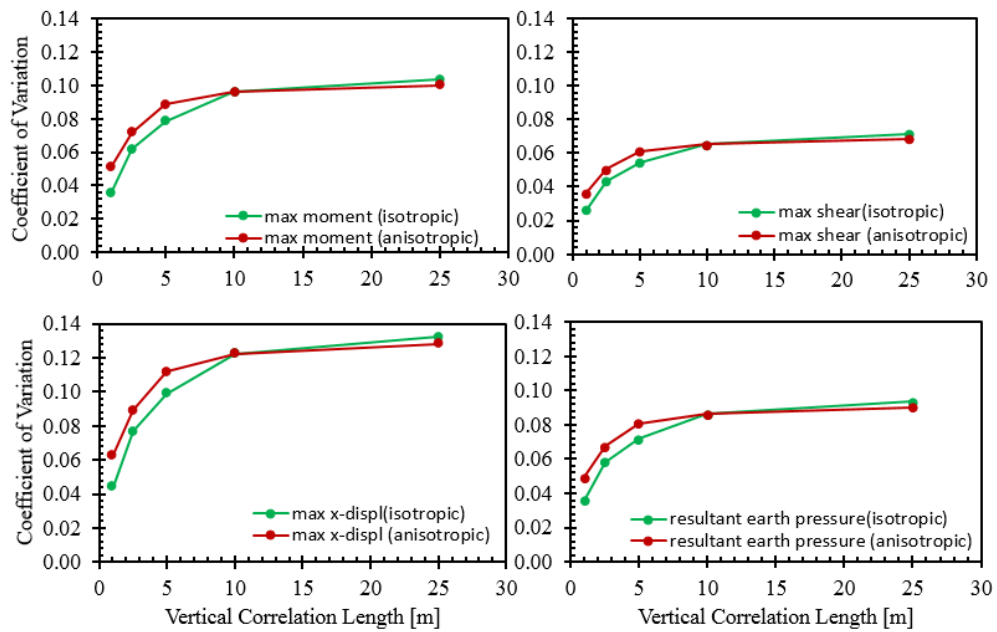
Figure 30. Variation of COV of Maximum Moment, Maximum Shear, Maximum x-Displacement, and Lateral Earth Pressure With The Vertical Correlation Length ($\mu (\varphi)$ = 33º, COV (tan φ) = 0.1)

The simulations were also repeated for different variabilities in the friction angle (COV (tan φ)= 5, 10, 15, 20%). Figure 31 presents the variation of the COVs of the four outputs for the isotropic and anisotropic case. For the anisotropic case, the horizontal and vertical correlation lengths are fixed at 10m and 1m respectively (θ_h = 10, θ_{v}= 1m). For the isotropic case the horizontal and vertical correlation lengths are fixed at 1m (θ_h = θ_{v}= 1m). It can be observed from Figure 31 that for the same vertical correlation lengths, the values of COV of all output for the case of anisotropic are higher than those of isotropic case. This can be traced to the averaging effect taking place in both directions in the isotropic case.
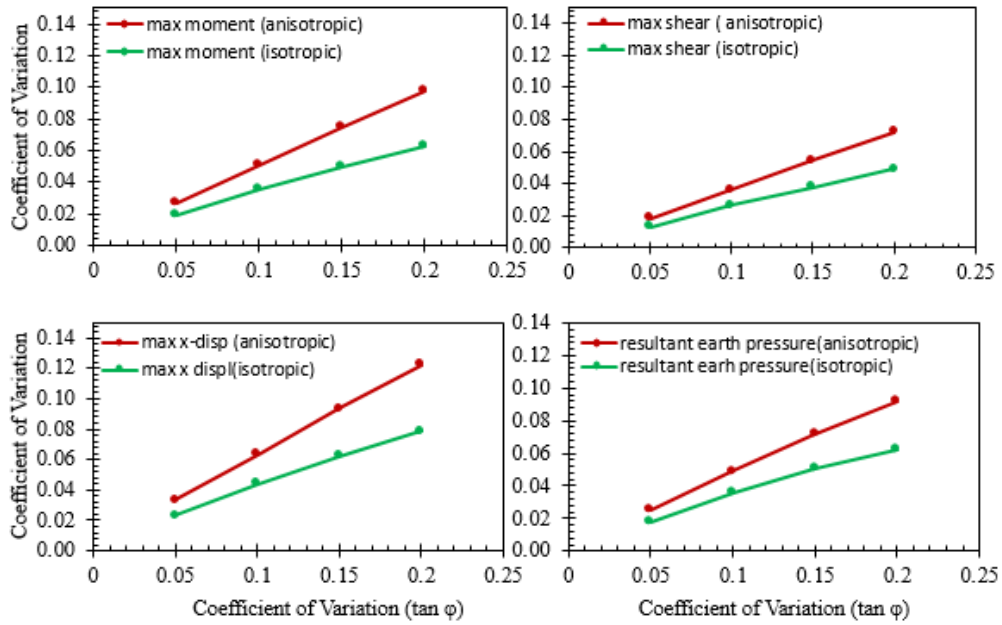
Figure 31. Variation of COV of Maximum Moment,Maximum Shear, Maximum X-Displacement, and Lateral Earth Pressure With The COV(tan φ)(μ (φ) = 33º)

5.3.2 Effect of backfill friction angle

Simulations were conducted for means of φ that are equal to 30°, 33° and 36° considering anisotropic friction angle with a horizontal correlation angle of 10m, in order to investigate the effect of the mean of the friction angle on the four outputs. The COV (tan φ) was fixed at 0.1. The values of the maximum moment and maximum shear are plotted for different vertical correlation lengths in Figure 32. The deterministic values are also plotted for comparison.

43
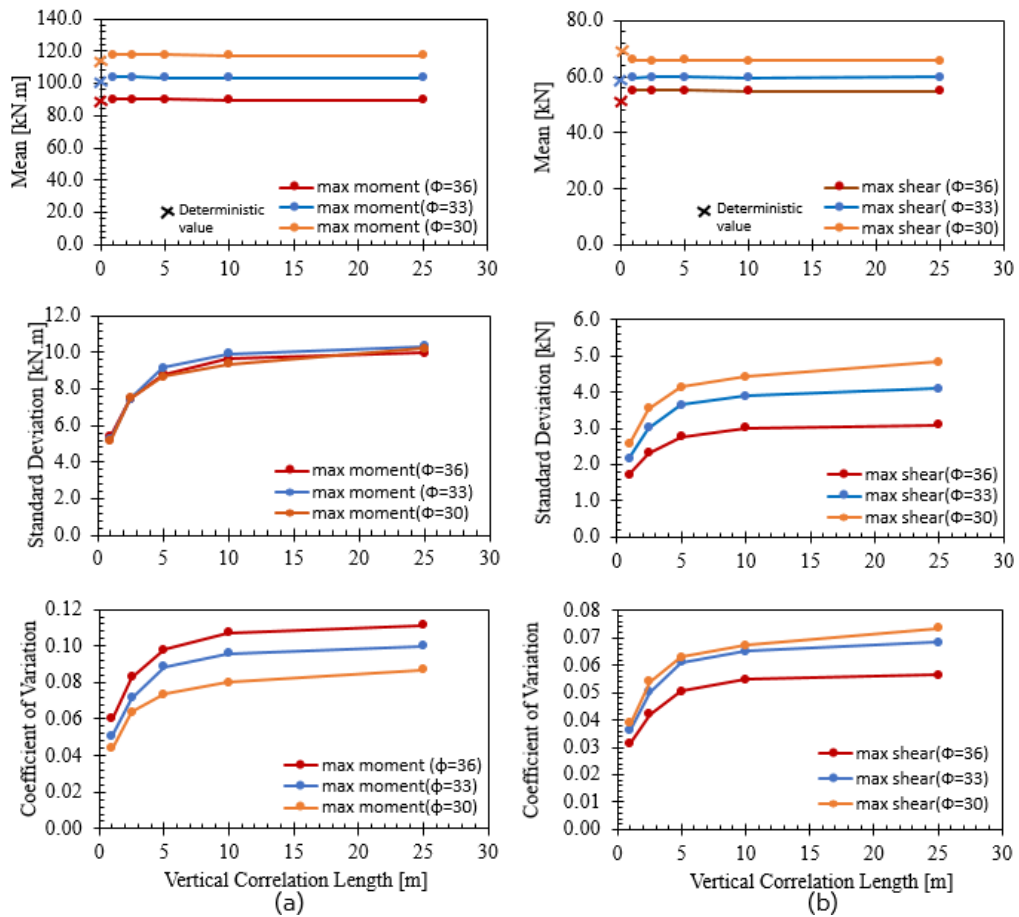
Figure 32. Variation of The Mean, STD, and COV Of (a) Maximum Moment, And (b) Shear Forces With The Vertical Correlation Length for Different Friction Angle Means for φ=30, 33, 36 (COV (tan φ) =0.1)

The results indicate that the mean of the maximum moment decreases when the mean of friction angle increases from 30 to 36, since the lateral earth pressure decreases as will be shown in Figure 33. The drop in the mean of the lateral pressure is due to the fact that when the friction between the particles increases the soil body can hold itself more, reducing the lateral stress on the wall. It can be seen that the STD of the maximum moment are not affected by the friction angle for all correlation lengths. As a result, the COV of the moment increases when the mean of φ increases since the mean decreases and the STD is constant.

The mean of the maximum shear force also decreases as the mean of the friction angle increases from 30 to 36 degrees. Unlike the bending moment, the STD of

the shear decreases with increase in backfill density. As a result, the COV in the

maximum shear seems to be less sensitive to changes in the friction angle of the soil.
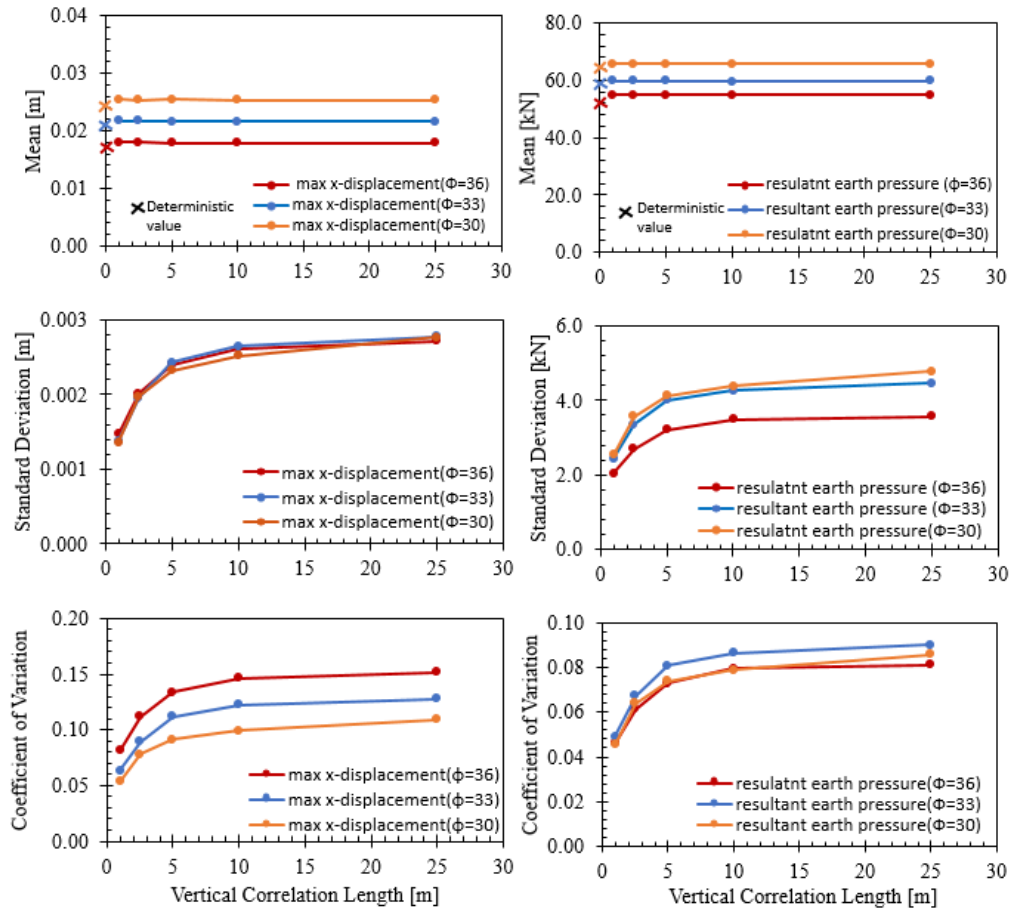
Figure 33. The Variation of The Mean, STD, and COV Of (A) The Maximum Horizontal Displacement(M), and (B) The Resultant Lateral Force(KN) With The Vertical Correlation Length for φ=30,33,36 (COV (tan φ) =0.1).

Figure 33 illustrates the variation of the mean, STD, and COV of the maximum

horizontal displacement and the resultant lateral force with the vertical correlation

length for φ=30, 33, and 36°.

As was seen for the case of the moment, the mean of maximum displacement decreases

when the mean of friction angle increase. Since the STD of maximum displacement is

approximately the same for the three friction angles, the COV increases when the mean

of φ increases. On the other hand, the response of the resultant lateral earth force is

similar to that of the maximum shear with reductions in the mean of the resultant earth pressure with increases in the friction angle, and a COV that is more-or-less insensitive to changes in the friction angle.

5.3.3   Lateral earth pressure for different θ_v and COV

In an effort to investigate the effect of the spatial variability of the friction angle on the lateral earth pressure behind the wall, many simulations were conducted for different COV and vertical correlations lengths.

Figure 34 shows the lateral earth pressure from 1600 realizations for the anisotropic spatial variability case. Four correlation lengths were considered: 1, 2.5, 5, and 10m. The COV (tan φ) was fixed at a constant value equal to 0.1. It is observed that the lateral earth pressure increases roughly in a linear trend from the top of the wall. A sharp peak appears near the base of the wall. This peak may be explained by the fact that the lower soil did not reach the active state yet. The pressure drops back due to the development of friction at the interface between the soil and wall base. The deterministic value of active lateral earth pressure is calculated for the three models developed by: Rankine, Coulomb, and Lancelotta. The dotted line displays the variation of earth pressure with the depth according to Rankine which is the critical value (largest). This line lies approximately at the 33% percentile of the generated realizations for all correlation lengths.

An investigation of the lateral earth pressure profiles in Figure 33 points to the importance of the correlation length of the friction angle of the backfill on the results. For the case with the smallest correlation length of 1.0m, the lateral pressure profiles with depth can be seen to be erratic and are seen to mix with each other for the different

46

realizations. Conversely, for the case involving the largest correlation length of 10m, the lateral earth pressure profiles from the different realizations can be distinguished from each other, with some profiles being at the lower end of the lateral stress spectrum and other profiles in other realizations being at the higher end of the spectrum, irrespective of the depth. This response is expected to govern the coefficients of variation in the output parameters including displacement, moment, and shear.
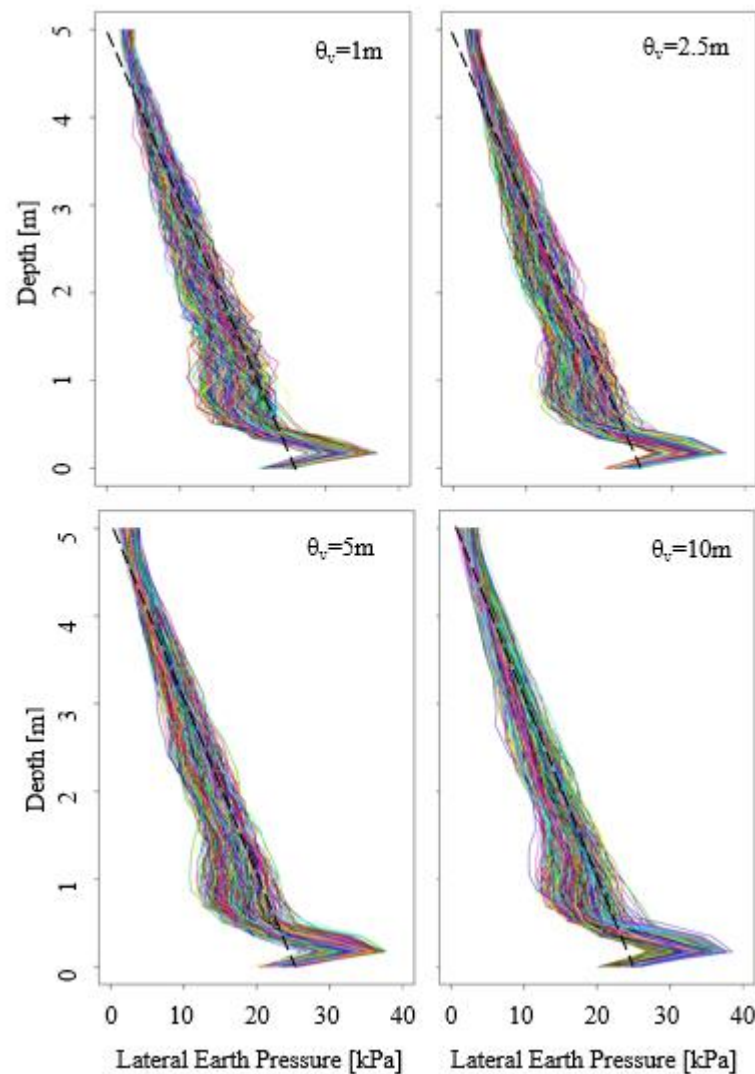
Figure 34. Lateral Earth Pressure for Different Vertical Correlation Lengths (μ (φ) = 33°, θ_h=10, COV (tan φ) =0.1)

The analysis is repeated for different COVs for the backfill friction angle in

order to study the effect of the uncertainty in the backfill friction angle on the

uncertainty in the resulting lateral earth profiles with depth. Figure 35 shows the lateral

earth pressure profiles from 1600 realizations for COV (tan φ) =0.05, 0.1, 0.15, and 0.2.

All these cases have a vertical correlation length that is equal to 1m and a horizontal

correlation length of 10m. It is clear from Figure 35 that the band of realizations widens

as the COV (tan φ) increases. This is because the lateral earth pressure is very sensitive

to the backfill friction angle. Thus, the variation in the outputs increases as the COV

(tan φ) increases.

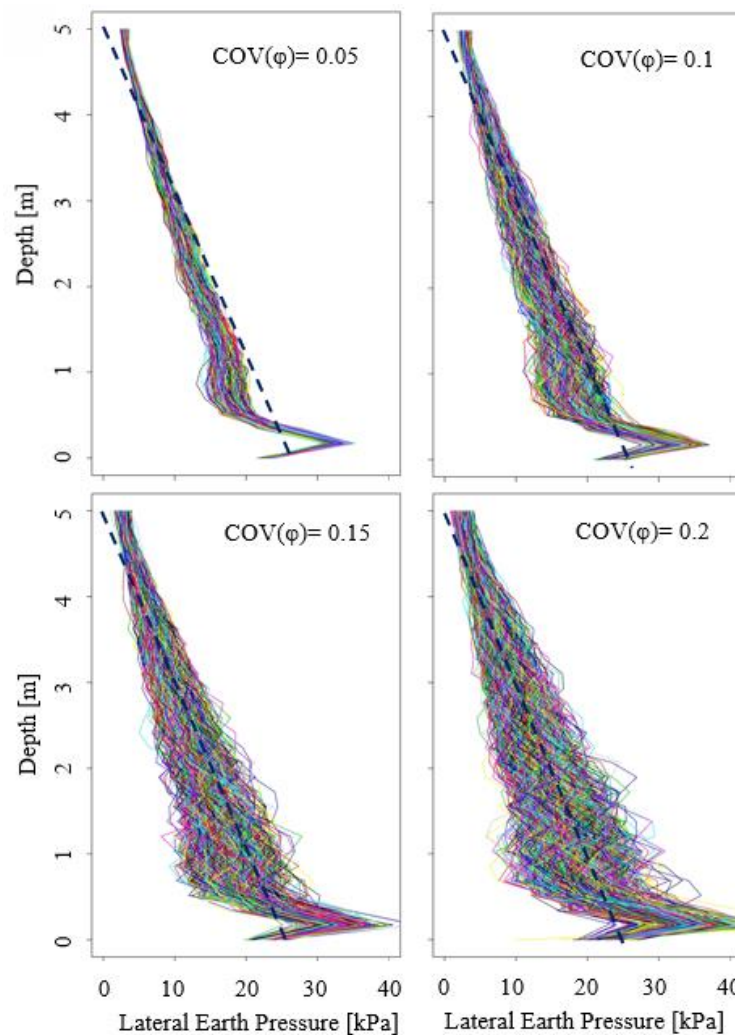
Figure 35. Lateral Earth Pressure for Different COVs (μ (φ) = 33°, θ_h=10, θ_v=1)

The results of all the numerical analyses are summarized in Table 7 (mean

48

values), Table 8 (standard deviations), and Table 9 (coefficients of variation) for all output variables.

Table 7. Summary of The Mean of Outputs for All Cases

Mean (φ)	COV $(\tan \varphi)$	Type of spatial variability	θ_h (m)	θ_v (m)	mean max moment (kN.m)	mean max shear (kN)	mean max x-disp.(m)	mean resultant lateral force (kN)
33	0.1	anisotropic	10	1	103.8	59.7	0.0217	59.5
33	0.1	anisotropic	10	2.5	104.0	59.9	0.0218	59.6
33	0.1	anisotropic	10	5	103.7	59.8	0.0217	59.5
33	0.1	isotropic	10	10	103.4	59.7	0.0216	59.4
33	0.1	anisotropic	10	25	103.6	59.8	0.0216	59.5
33	0.1	isotropic	1	1	104.1	59.9	0.0218	59.5
33	0.1	isotropic	2.5	2.5	103.7	59.8	0.0217	59.6
33	0.1	isotropic	5	5	103.5	59.7	0.0216	59.5
33	0.1	isotropic	25	25	103.6	59.8	0.0217	59.5
33	0.05	anisotropic	10	1	103.2	59.3	0.02154	59.0
33	0.15	anisotropic	10	1	104.7	60.3	0.02192	60.0
33	0.2	anisotropic	10	1	106.4	61.3	0.02239	60.8
33	0.05	isotropic	1	1	103.2	59.3	0.0215	59.1
33	0.15	isotropic	1	1	105.6	60.9	0.0221	60.5
33	0.2	isotropic	1	1	107.5	62.2	0.0226	61.5
36	0.1	anisotropic	10	1	90.3	55.0	0.0180	55.1
36	0.1	anisotropic	10	2.5	90.1	55.0	0.0180	55.1
36	0.1	anisotropic	10	5	90.0	55.0	0.0179	55.1
36	0.1	isotropic	10	10	89.7	55.0	0.0179	55.0
36	0.1	anisotropic	10	25	89.7	55.0	0.0179	55.0
30	0.1	anisotropic	10	1	117.7	65.9	0.0254	65.8
30	0.1	anisotropic	10	2.5	117.5	65.8	0.0254	65.8
30	0.1	anisotropic	10	5	117.6	65.9	0.0254	65.8
30	0.1	isotropic	10	10	117.1	65.8	0.0253	65.6
30	0.1	anisotropic	10	25	117.2	65.8	0.0253	65.7

Table 8. Summary of STD of Outputs for All Cases

Mean (φ)	COV (tan φ)	Type of spatial variability	θ_h (m)	θ_v (m)	STD max moment (kN.m)	STD max shear(kN)	STD Max x-disp.(m)	STD resultant lateral force(kN)
33	0.1	anisotropic	10	1	5.3	2.2	0.0014	2.4
33	0.1	anisotropic	10	2.5	7.5	3.0	0.0019	3.3
33	0.1	anisotropic	10	5	9.2	3.6	0.0024	4.0
33	0.1	anisotropic	10	10	9.9	3.9	0.0026	4.3
33	0.1	anisotropic	10	25	10.4	4.1	0.0028	4.5
33	0.1	isotropic	1	1	3.7	1.6	0.0010	1.8
33	0.1	isotropic	2.5	2.5	6.4	2.6	0.0017	2.9
33	0.1	isotropic	5	5	8.1	3.2	0.0021	3.6
33	0.1	isotropic	25	25	10.7	4.3	0.0029	4.6
33	0.05	anisotropic	10	1	2.8	1.1	0.0007	1.3
33	0.15	anisotropic	10	1	7.8	3.3	0.0020	3.6
33	0.2	anisotropic	10	1	10.4	4.4	0.0027	4.7
33	0.05	isotropic	1	1	1.9	0.8	0.0005	1.0
33	0.15	isotropic	1	1	5.3	2.3	0.0014	3.0
33	0.2	isotropic	1	1	6.8	3.0	0.0018	3.9
36	0.1	anisotropic	10	1	7.8	3.3	0.0020	3.6
36	0.1	anisotropic	10	2.5	10.4	4.4	0.0027	4.7
36	0.1	anisotropic	10	5	8.8	2.8	0.0024	3.2
36	0.1	isotropic	10	10	9.6	3.0	0.0026	3.5
36	0.1	anisotropic	10	25	10.0	3.1	0.0027	3.6
30	0.1	anisotropic	10	1	5.2	2.6	0.0014	2.5
30	0.1	anisotropic	10	2.5	7.5	3.6	0.0020	3.6
30	0.1	anisotropic	10	5	8.7	4.2	0.0023	4.1
30	0.1	isotropic	10	10	9.4	4.4	0.0	4.4
30	0.1	anisotropic	10	25	10.2	4.8	0.0	4.8

Table 9. Summary of COV of outputs for all cases

Mean (φ)	COV (tan φ)	Type of spatial variability	θ_h (m)	θ_v (m)	COV max moment	COV max shear	COV max x-disp.	COV resultant lateral force
33	0.1	anisotropic	10	1	0.051	0.036	0.063	0.049
33	0.1	anisotropic	10	2.5	0.072	0.050	0.090	0.067
33	0.1	anisotropic	10	5	0.088	0.061	0.112	0.081

33	0.1	isotropic	10	10	0.096	0.065	0.122	0.086
33	0.1	anisotropic	10	25	0.100	0.069	0.128	0.090
33	0.1	isotropic	2.5	2.5	0.062	0.043	0.077	0.058
33	0.1	isotropic	5	5	0.078	0.054	0.099	0.072
33	0.1	isotropic	25	25	0.103	0.071	0.133	0.093
33	0.05	isotropic	1	1	0.019	0.013	0.023	0.018
33	0.1	isotropic	1	1	0.035	0.026	0.044	0.036
33	0.15	isotropic	1	1	0.050	0.038	0.062	0.050
33	0.2	isotropic	1	1	0.063	0.049	0.079	0.062
33	0.05	anisotropic	10	1	0.027	0.019	0.033	0.026
33	0.15	anisotropic	10	1	0.075	0.054	0.093	0.072
33	0.2	anisotropic	10	1	0.098	0.072	0.122	0.092
36	0.1	anisotropic	10	1	0.060	0.031	0.081	0.046
36	0.1	anisotropic	10	2.5	0.083	0.042	0.112	0.061
36	0.1	anisotropic	10	5	0.098	0.051	0.133	0.073
36	0.1	isotropic	10	10	0.107	0.055	0.146	0.079
36	0.1	anisotropic	10	25	0.111	0.057	0.152	0.081
30	0.1	anisotropic	10	1	0.044	0.039	0.054	0.046
30	0.1	anisotropic	10	2.5	0.064	0.054	0.078	0.061
30	0.1	anisotropic	10	5	0.074	0.063	0.091	0.073
30	0.1	isotropic	10	10	0.080	0.067	0.099	0.079
30	0.1	anisotropic	10	25	0.087	0.074	0.109	0.081

Chapter 6

IMPLICATIONS ON STRUCTURAL DESIGN OF WALL USING EC7

6.1 Introduction

In the previous sections, the variability in the load demand (shear and moment) on a cantilever wall that is supporting a random cohesionless backfill was quantified. In this section, analytical models for the shear resistance and moment resistance of the wall are used to calculate the probability of failure for these two limit states (shear failure and flexural failure) based on the Eurocode recommended partial factors. Additionally, new partial factors are proposed to meet the target probabilities of failure for different reliability classification in compliance with the Eurocode.

6.2 Design for Flexure

After checking the stability of the wall against the three failure modes (sliding, overturning, and bearing capacity), a structural design is needed to calculate the steel reinforcement to cater for the moment demand. The equation proposed by Eurocode is:

$$A_s = \frac{M_R}{0.87 \times f_y \times Z} \tag{12}$$

$$Z = d \times \left(0.5 + \sqrt{0.25 - \frac{k_m}{1.134}} \right) \tag{13}$$

$$k_m = \frac{M_L}{(b \times d^2 \times f_{ck})} \tag{14}$$

M_R is the resistance moment, M_L is the loading moment, b is the wall section width, and d is the effective depth. An equation of M_R can be extracted from the three above equations such that:

$$M_R = A_s \times 0.87 \times f_y \times d \times \left(0.5 + \sqrt{0.25 - \frac{\frac{M_L}{(b \times d^2 \times f_{ck})}}{1.134}} \right) \tag{15}$$

In the structural reliability analysis, f_y and f_{ck} are assumed to follow a lognormal distribution with mean values of 455 and 31MPa respectively and a COV of 0.05. A_s, b and d are assumed to have deterministic values that are given in the deterministic analysis.

The performance function that is needed to define failure is then given by the equation:

$$g = M_R - M_L = A_s \times 0.87 \times f_y \times d \times \left(0.5 + \sqrt{0.25 - \frac{\frac{M_L}{(b \times d^2 \times f_{ck})}}{1.134}} \right) - M_L \tag{16}$$

In order to calculate the probability of failure of the wall in the flexural mode, the probability distribution of M_L needs to be defined. Figure 36 shows a Q-Q plot for the logarithm of M_L as obtained from the 1600 random field realizations for a typical case involving $\mu(\varphi) = 33°$, COV($\tan\varphi$) = 0.1, $\theta_h = 10$, and $\theta_v = 1$. The Q-Q plot shows that the logarithm of (M_L) can be assumed to follow a normal distribution. Similar results were obtained for other cases indicating that M_L could be realistically modelled by a

lognormal distribution in the structural reliability analysis. Monte Carlo Simulations with 10,000,000 realizations were used to calculate the probability of failure defined as the number of cases where the performance function in equation 16 results in negative values divided by the total number of realizations. The number of simulated realizations is calculated from:

$$N = \left(\frac{196}{error}\right)^2 \times \frac{(1-p)}{p} \tag{17}$$

The calculation is done with 95% confidence for an estimated probability of failure of 0.005% with a percent error of 5%.
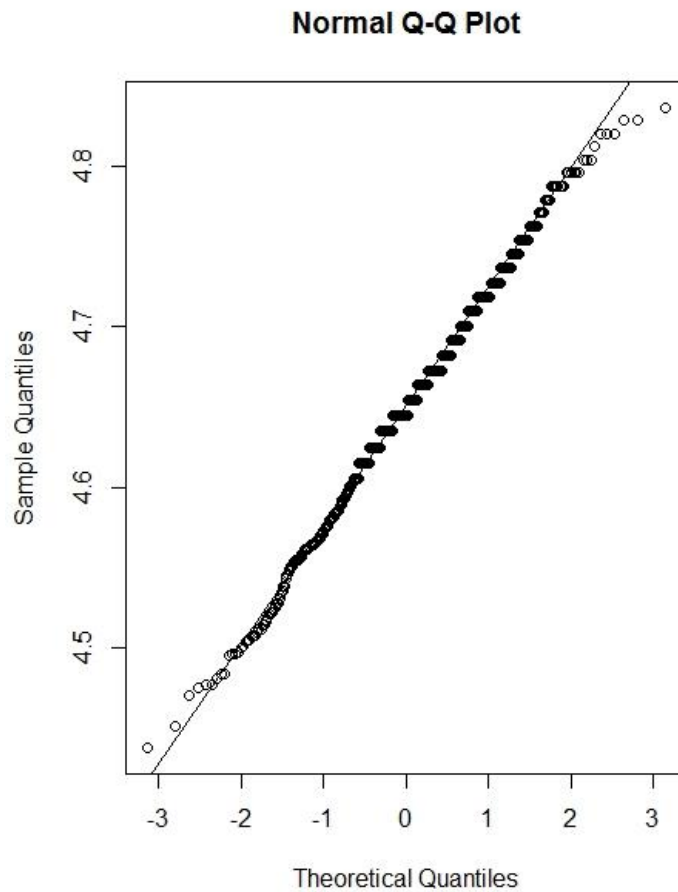
Figure 36. Q-Q plot of ln (M_L) (μ (φ) = 33°, COV (tan φ) = 0.1, θ_h=10, and θ_v=1)

The recommended minimum values for the reliability index β for ultimate limit states proposed by Eurocode 7 are given in   Table 10. The probabilities of failure for the three reliability indices are also shown in the Table. RC1, RC2, and RC3 are the three reliability classes of the Eurocode.

RC3: high consequences of failure.

RC2: medium consequences of failure.

RC3: low consequences of failure.

Table 10. Recommended Minimum Values for Reliability Index B

Reliability Class	Minimum value for β for 50 years reference period	Probability of failure
RC3	4.3	8.54E-06
RC2	3.8	7.23E-05
RC1	3.3	4.83E-04

Reliability analyses were conducted for cases involving random fields with different friction angles and different correlation structures for the friction angle of the backfill. For each case analyzed, the area of steel reinforcement in the wall was calculated based in Eurocode 7 and the probability of failure against flexural failure was calculated using the performance function in equation 16. The resulting probabilities of failure are plotted as a function of the vertical correlation length in Figure 36 for the cases with φ=30, 33, and 36°, COV (tan φ) =0.1, and θ_h=10m. Also shown on Figure 36 are the three target reliability indices that are specified by Eurocode 7.

The first observation from Figure 37 is that the probability of failure for the flexural mode of failure of the wall increases as the correlation length increases,

irrespective of the density of the backfill. These results are expected since the COV of

the maximum moment that acts on the wall was shown to increase with the correlation

length. The second observation from Figure 36 is that the probability of failure increases

with an increase in the friction angle of the backfill for any given correlation length.

This trend correlates well with the trend observed for the COV of the maximum

moment which was shown in Figure 32 to increase with friction angle. It should be

noted however that the probabilities of failure that were calculated for the case with a

friction angle of 30 were much smaller than those observed for the cases with $\varphi = 33$

and 36 degrees. This nonlinearity in the relationship between the probability of flexural

failure and the friction angle of the backfill soil is related to the nonlinear performance

function in which the uncertain maximum moment in the wall M_L shows up in both the

load and the resistance components in equation 16. Since the mean and COV of the

maximum moment M_L are governed by the density of the backfill, the probability of

failure in the flexural model ends up being a non-linear function of the density of the

backfill as indicated in Figure 32.

The third observation from Figure 32 is that the use of the Eurocode-

recommended partial factors results in probabilities of failure that vary in a wide range

depending on the mean value and correlation length of the friction angle of the backfill.

For example, the cases involving loose backfill with a mean friction angle of 30º

resulted in probabilities of failure that are smaller than the target probabilities of failure

recommended in Eurocode, irrespective of the reliability classification level (RC1 to

RC3) and irrespective of the correlation length assumed. For the cases involving the

denser backfill (mean friction angles of 33 and 36 degrees), the resulting probabilities of

failure were all greater than that allowed for RC3, except for cases involving correlation lengths that are smaller than 2.5m. For cases with correlation lengths that are greater than 2.5m, the probabilities of failure increase and approach the Eurocode target reliability index for RC2 for cases with correlation lengths of 5m, and exceed the target reliability index for RC2 for cases with correlation lengths exceeding 10m. It should be noted that all analyzed cases resulted in probabilities of failure that were within those allowed by Eurocode for reliability classification RC1.
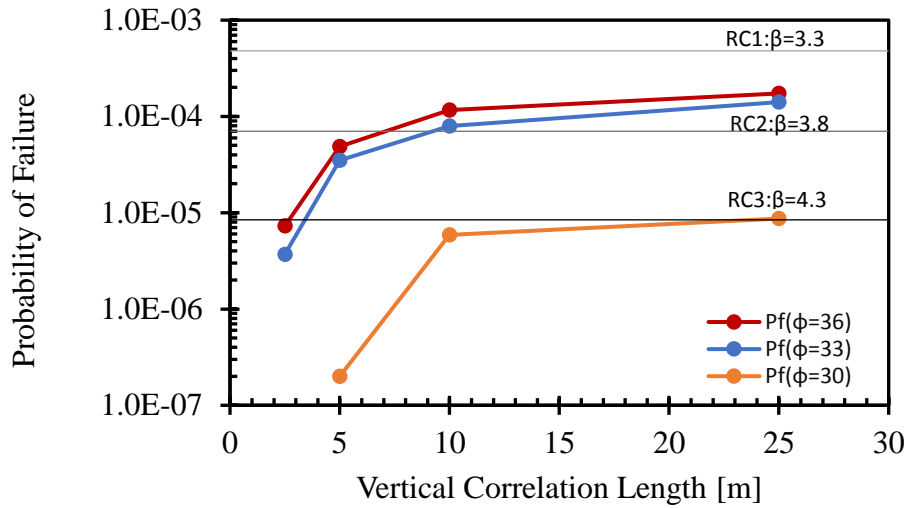
Figure 37. Variation of The Probability of Failure In Flexure With The Vertical Correlation Length for φ =30, 33, and 36°(COV (tan φ) =0.1,θ$_h$=10m.)

6.3 Design for shear

The same analysis is done for the shear force. The equation proposed by Eurocode is:

$$V = 0.12 \times K_v \times b \times d \times (100 \times f_{ck} \times \rho)^{\frac{1}{3}} \tag{18}$$

where $K_v = 1 + \sqrt{\frac{200}{d}}$, and $\rho = \frac{A_s}{b \times d}$

The performance function is then given by the equation $h = V_R - V_L$

Where V_L is random maximum shear force that is based on the random field modeling of the wall in FLAC® and V_R is obtained from the following equation:

$$V_R = 0.12 \times K_v \times b \times d \times (100 \times f_c \times \rho)^{\frac{1}{3}} \tag{19}$$

The results show that the probability of failure for the case of shear is very small compared to that for the bending moment for all cases, which indicates that the design is very safe for shear. Therefore, the focus in the rest of the study will be on the flexural response.

6.4 Recommended partial factors for Eurocode 7

Since the probability of failure depends on the correlation length, mean friction angle, and COV (tan φ), the reliability analysis could be used to recommend partial factors that would result in probabilities of failure that meet the three reliability classifications given in the Eurocode. To achieve this objective, the probability of failure corresponding to a range of partial factors between 0.9 and 1.6 is calculated for the studied cases. For illustration, Figure 38 displays the variation of the probability of failure with respect to the assumed partial factor for different COV (tan φ) for the case when $\mu(\varphi) = 33^\circ$, θ_h=10m, and θ_v= 1m. The probability of failure for the three reliability classifications of the Eurocode as well as the recommended partial factors are also shown for comparison.
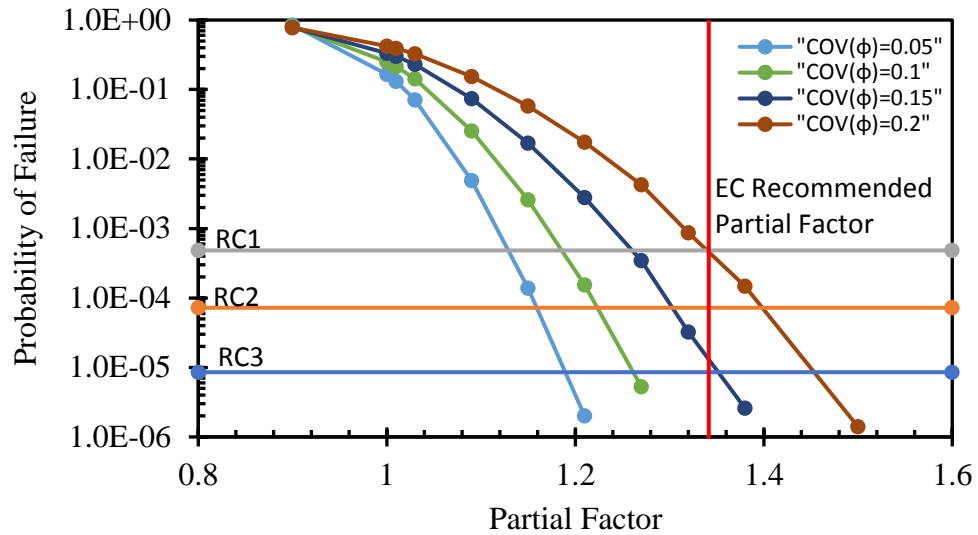
Figure 38. Variation of The Probability of Failure With The Partial Factors for Different COVs ($\mu(\varphi)$=33°, θh=10, and θv=1)

It is clear from Figure 38 that the probability of failure decreases when the partial factor increases. For COV (tan φ) < 0.15, the design using the current Eurocode-recommended partial factor is safe for all levels of reliability classifications (RC1 to RC3). For COV (tan φ) = 0.2, the probabilities of failure are relatively higher and a revised partial factor of 1.45 is necessary to meet the reliability classification RC3. Results on Figure 37 indicate that reductions in the recommended Eurocode partial factors could be implemented for cases involving lower variability in the friction angle of the backfill. For example, for cases with a COV (tan φ) = 0.05, a partial factor of 1.2 is enough to meet the reliability classification 3 (lowest probability of failure). For COV (tan φ) = 0.1, a partial factor of 1.3 is needed.

In order to investigate the effect of the correlation length on the required partial factors, the analysis involving the base case with a μ (φ) = 33°, COV(tan φ)= 0.1, and θ_h=10m was repeated for different correlation lengths. Figure shows the variation of the partial factors required to produce probabilities of failure that are consistent with the three target reliability classification levels in Eurocode.

Results on Figure 39 indicate that for a target β of 4.3 (RC3), the required partial factors increase from 1.26 to 1.5 when the vertical correlation length of the friction angle random field increases from 1 to 25m. The same trend is observed for RC2 (β=3.8) with relatively lower required partial factors ranging from 1.2 to 1.38. For the lowest reliability classification level RC1 (β=3.3), the partial factors decrease to reach a value of 1.15 for a vertical correlation length of 1m and 1.32 for a vertical correlation length of 25m. It can be deduced that for β=3.3, all partial factor values are smaller than the value proposed by Eurocode. For β=3.8, values that are smaller than 1.35 are required for low vertical correlation lengths ($\theta_v < 10$) and greater than this value for high vertical correlation lengths ($\theta_v > 10$). Finally, for β=4.3, partial factors less than 1.35 are required for $\theta_v < 5$ and greater than this value for $\theta_v > 5$.
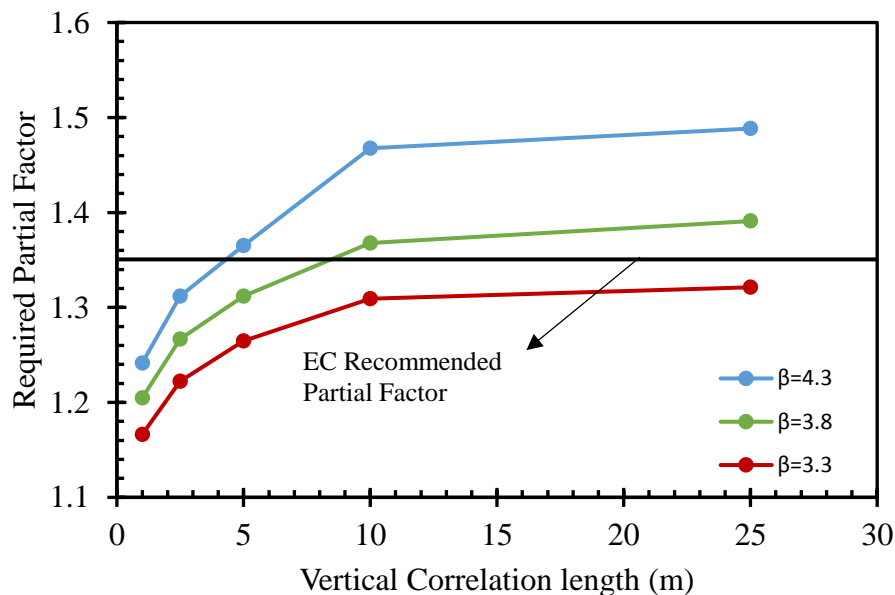
Figure 39. Variation of Partial Factor With The Vertical Correlation Length [M] for Anisotropic Case (μ (φ) = 33º ,COV(tan φ)= 0.1, θ_h=10)

The analysis is repeated for different values of COV (tan φ). The variation of the required partial factor with the coefficient of variation for anisotropic case ((μ (φ) =

33º, θ_v=1, θ_h=10) is plotted in Figure 40. The results show an increase in the partial factor when the COV (tan φ) increases from 0.05 to 0.2, for the three βs to reach a maximum value of 1.5 for β= 4.3 (COV (tan φ) =0.2). For β= 3.3, the values of partial factor are smaller than 1.35 for four the COV (tan φ). For β= 3.8 and β= 4.3, partial factors less than 1.35 are required for COV (tan φ) < 0.15 and greater than this value for COV (tan φ) > 0.15.
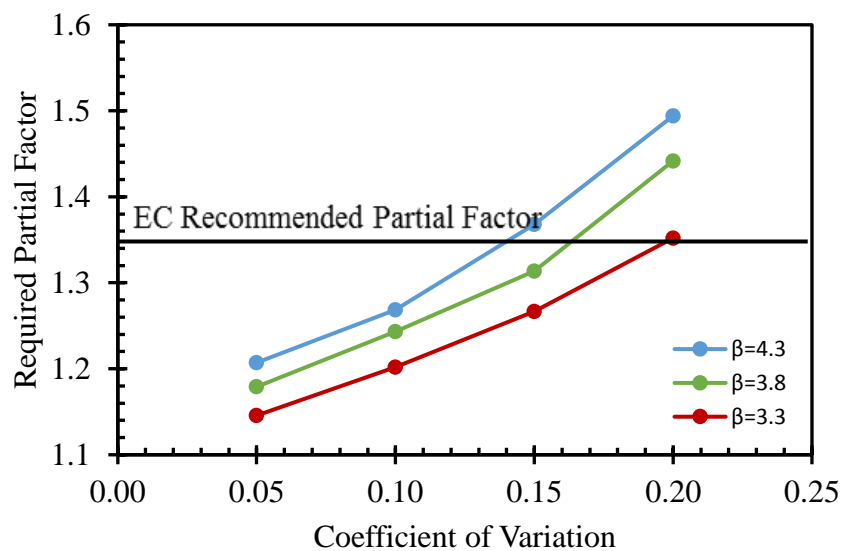
Figure 40. Variation of Partial Factor With The Coefficient of Variation for The Anisotropic Case ($\mu(\varphi) = 33º$, θv=1, θh=10)

The recommended partial factors that are displayed in Figures 39 correspond to cases involving an anisotropic random field of the friction angle for the backfill soil with a horizontal correlation length of 10m and varying vertical correlation lengths. Although the anisotropic random field of φ is expected to be a more realistic representation of reality than an isotropic random field, a comparison between the required partial factors for the two types of spatial variability could be of significance. Such a comparison is displayed in Figure 41.
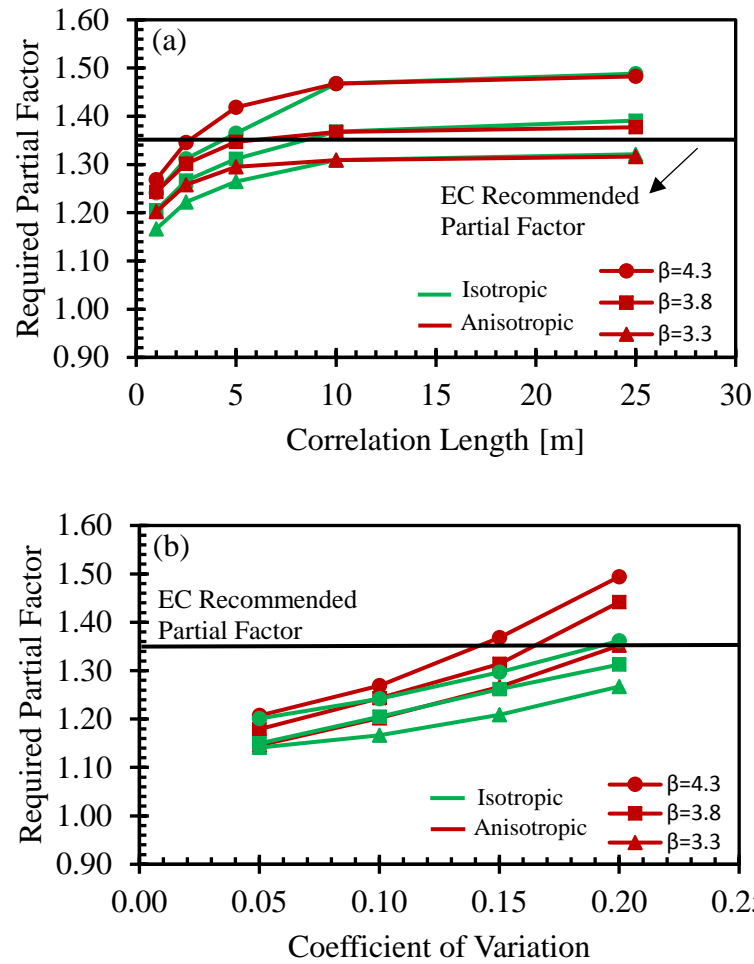
Figure 41. Variation of Partial Factor With (a) The Vertical Correlation Length((μ (φ) = 33º , θh=10, COV (tan φ)=0.1),and With (b) the COV(tan φ) ($\mu(\varphi)$=33º , θv =1, θh=10(Anisotropic Case))

Figure 41 shows the variation of the recommended partial factors for the three target reliability indices with the correlation length (Figure 41a) and COV (tan φ) (Figure 41b). For any given vertical correlation length that is less than 5.0m, it can be observed from Figure 41a that the partial factors for the anisotropic spatial variability are slightly larger than those of the isotropic case, a response that is compatible with results obtained in the previous sections. For correlation lengths that are larger than 5.0m, the calculated partial factors are identical in the two cases considered. Considering different COVs of φ, the curves on Figure 41b also show that the required partial factors for the anisotropic spatial variability are greater than those of the isotropic

case for the three target reliability indexes. The difference between the required partial factors can be observed to increase as the COV of the friction angle increases. It is interesting to note that for the specific cases considered in Figure 41b ($\mu(\varphi)=33^\circ$, θ_v =1m), the current Eurocode partial factor is capable of ensuring reliability levels that are consistent with the three target reliability classification s(RC1 to RC3). This conclusion does not hold for the equivalent anisotropic cases, which show the need for the use of larger partial factors, particularly for COVs of φ exceeding 0.15.

Figure 42 portrays the effect of the mean of the friction angle on the required partial factors for the three target reliability indices. It is observed that the partial factors vary non-linearly with the mean of φ for the three reliability indexes proposed by Eurocode. As the mean of friction angle increase from 30 to 33 the values of partial factors increase. These values drop when the friction angle increases to 36. Results on Figure 41 indicate that for the lowest reliability classification RC1 ($\beta=3.3$), the current Eurocode partial factor is adequate irrespective of the density of the sand backfill and irrespective of the correlation length. For the intermediate reliability classification RC2 ($\beta=3.8$), partial factors that are slightly greater (~ 1.40) than the Eurocode factor of 1.35 are needed to maintain the target reliability index for cases with correlation lengths that are greater than 5.0 m. For smaller correlation lengths, the current Eurocode factor is considered adequate, irrespective of the friction angle of the sand. For the most stringent reliability classification RC3 ($\beta=4.3$), partial factors that are greater than 1.35 are required starting from $\theta_v>2.5$m for $\varphi=33$ and 36°. A recommended partial factor of 1.50 will satisfy the target reliability level for all correlation lengths and for all sand densities.
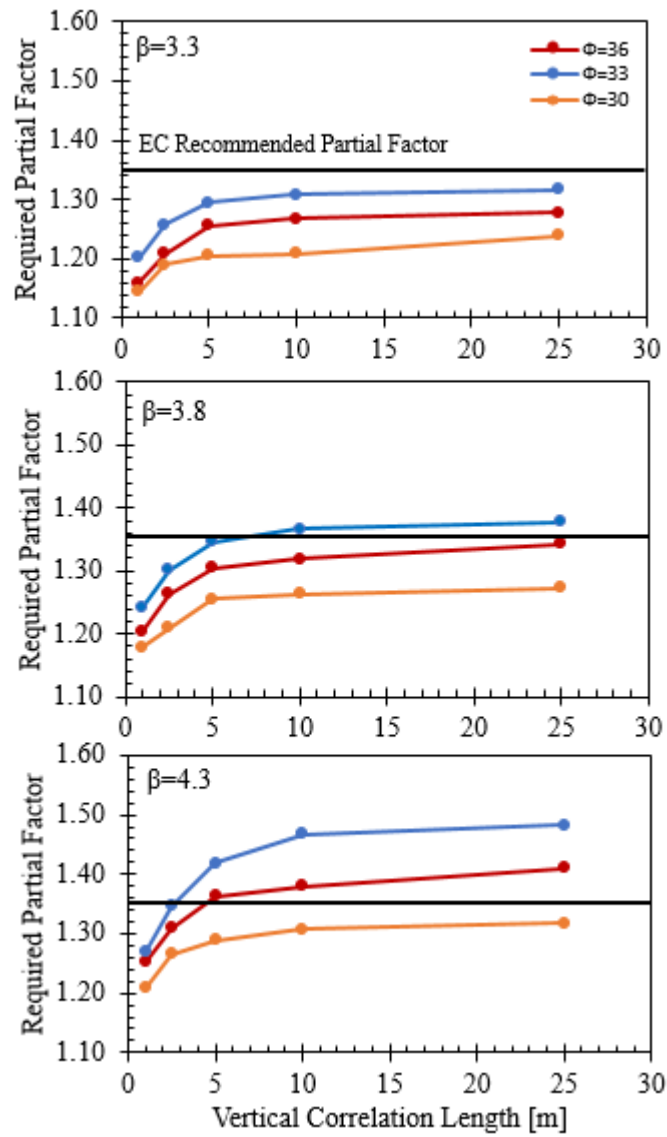
Figure 42. Variation of Partial Factor With The Vertical Correlation Length for Different Friction Angle (Anisotropic Case: COV (φ)=0.1, θh=10)

CHAPTER 7

CONCLUSIONS

This study uses the random finite difference method implemented in FLAC 2D® to investigate the effect of the spatial variability of the backfill soil on the structural response of the wall. The friction angle of backfill soil is the only source of uncertainty that was incorporated in the analysis. The effect of different random field properties and soil parameters was analyzed to investigate the risk level that is inherent in the design of a cantilever retaining wall based on partial safety factor approaches proposed by Eurocode 7. The results allow designers to use a partial factor on the design according to the probability of failure.

The parameters that were varied are the friction angle of the backfill soil ranging from 30 to 36, the vertical and horizontal correlation lengths ranging from 1.0m to 25m, and the COV of the friction angle ranging from 0.05 to 0.2. Two types of spatial variability in the friction angle of the backfill soil were considered and compared: isotropic and anisotropic.

Based on the results, the following conclusions can be drawn:

1. The COV of the maximum moment, maximum shear, maximum displacement, and resultant earth pressure increase exponentially with the increase of vertical correlation length and linearly with the increase of COV (tan φ).

2. For different COV (tan φ) and different correlation lengths, the values of the COV of the maximum moment, maximum shear, maximum displacement, and resultant earth pressure of anisotropic spatial variability are higher than those of the isotropic case, particularly for smaller correlation lengths.

3. The scale of fluctuation of the lateral earth pressure increases as the vertical correlation length increases. The band of realizations of the lateral earth pressure widens as the COVs (tan φ) increase.

4. The partial factor (1.35) recommended by Eurocode 7 is insufficient for high COVs (tan φ) and high vertical correlation lengths. Results from the anisotropic random field with a horizontal correlation length of 10m indicate that for a target β=3.3, all recommended partial factor values are smaller than the value proposed by the Eurocode. For β=3.8, values that are smaller than 1.35 are required for low vertical correlation lengths (θ_v < 10) and greater than 1.35 for high vertical correlation lengths (θ_v > 10). Finally, for β=4.3, partial factors less than 1.35 are required for θ_v < 5 and greater than this value for θ_v > 5.

5. The partial factors for the anisotropic spatial variability are greater than those of isotropic case for small correlation lengths.

6. For the lowest reliability classification RC1 (β=3.3), the current Eurocode partial factor is adequate irrespective of the density of the sand backfill and irrespective of the correlation length. For the intermediate reliability classification RC2 (β=3.8), partial factors that are slightly greater ($\sim$ 1.40) than the Eurocode factor of 1.35 are needed to maintain the target reliability index for cases with correlation lengths that are greater than 5.0 m. For smaller correlation lengths, the current Eurocode factor is considered adequate, irrespective of the friction angle of the sand. For the most stringent reliability classification RC3 (β=4.3), partial factors that are greater than 1.35 are required starting from θv>2.5m for φ =33 and 36º. A recommended partial factor of 1.50 will satisfy the target reliability level for all correlation lengths and for all sand densities.

REFERENCES

Bond, A. J., Schuppener, B., Scarpelli, G., Orr, T. L., Dimova, S., Nikolova, B., & Pinto, A. V. (2013). Eurocode 7: geotechnical design worked examples. *In Workshop "Eurocode (Vol. 7).*

British Standard, B. S. 8110 (1997) Structural use of concrete-part 1. Code of practice for design and construction. British Standards Institution, London

Chalermyanont, T., & Benson, C. H. (2005). Reliability-based design for external stability of mechanically stabilized earth walls. *International Journal of Geomechanics*, *5*(3), 196-205.

Daryani, K. E., & Mohamad, H. (2014). System reliability-based analysis of cantilever retaining walls embedded in granular soils. *Georisk: Assessment and Management of Risk for Engineered Systems and Geohazards*, *8*(3), 192-201.

Dasgupta, U. S., Chauhan, V. B., & Dasaka, S. M. (2017). Influence of spatially random soil on lateral thrust and failure surface in earth retaining walls. *Georisk: Assessment and Management of Risk for Engineered Systems and Geohazards*, *11*(3), 247-256.

Dasgupta, U. S., Chauhan, V. B., & Dasaka, S. M. (2017). Influence of spatially random soil on lateral thrust and failure surface in earth retaining walls. *Georisk: Assessment and Management of Risk for Engineered Systems and Geohazards*, *11*(3), 247-256.

Duncan, J. M. (2000). Factors of safety and reliability in geotechnical engineering. *Journal of geotechnical and geoenvironmental engineering*, *126*(4), 307-316.

Fenton, G. A., Griffiths, D. V., & Williams, M. B. (2007). Reliability of traditional retaining wall design. In *Risk and Variability in Geotechnical Engineering* (pp. 165-172). Thomas Telford Publishing.

Goh, A. T., Phoon, K. K., & Kulhawy, F. H. (2009). Reliability analysis of partial safety factor design method for cantilever retaining walls in granular soils. *Journal of geotechnical and geoenvironmental engineering*, *135*(5), 616-622.

Griffiths, D. V., Fenton, G. A., & Ziemann, H. R. (2008). Reliability of passive earth pressure. *Georisk*, *2*(2), 113-121.

GuhaRay, A., Ghosh, S., & Baidya, D. K. (2014). Risk factor based design of cantilever retaining walls. *Geotechnical and Geological Engineering*, *32*(1), 179-189.

Itasca Consulting Group, Inc. 2016. *FLAC – Fast Lagrangian Analysis of Continua, Ver. 8.0 Theory and Background*. Minneapolis: Itasca.

Itasca Consulting Group, Inc. 2016. *FLAC – Fast Lagrangian Analysis of Continua, Ver. 8.0 User's Guide*. Minneapolis: Itasca.

Rahman, S., & Rao, B. N. (2001). A perturbation method for stochastic meshless analysis in elastostatics. *International Journal for Numerical Methods in Engineering*, *50*(8), 1969-1991.

Sayed, S., Dodagoudar, G. R., & Rajagopal, K. (2010). Finite element reliability analysis of reinforced retaining walls. *Geomechanics and Geoengineering: An International Journal*, *5*(3), 187-197.

Sert, S., Luo, Z., Xiao, J., Gong, W., & Juang, C. H. (2016). Probabilistic analysis of responses of cantilever wall-supported excavations in sands considering vertical spatial variability. *Computers and Geotechnics*, *75*, 182-191.

Shinozuka, M. and Yamazaki, F. (1988). Stochastic finite element analysis: an introduction, in Stochastic structural dynamics, (eds S. T.Ariaratnam, G. Schueller and I. Elishakoff), *New York,Elsevier Applied Science,* 243–290.

Sivakumar Babu, G. L., & Basha, B. M. (2008). Optimum design of cantilever retaining walls using target reliability approach. *International journal of geomechanics, 8(4),* 240-252.

Standard, B. (1986). Structural use of concrete. BS8110

Sujith, M., Menon, D., & Dodagoudar, G. (2011). Reliability analysis and design of cantilever RC retaining walls against sliding failure. *International Journal of Geotechnical Engineering, 5(2),* 131-141.

Threlfall, A. J. (2013). Worked Examples for the Design of Concrete Structures to Eurocode 2. CRC Press.

Zevgolis, I. E., & Bourdeau, P. L. (2010). System reliability analysis of the external stability of reinforced soil structures. *Georisk, 4(3),* 148-156.

Zhang, D. B., Sun, Z. B., & Zhu, C. Q. (2013). Reliability analysis of retaining walls with multiple failure modes. *Journal of Central South University, 20(10),* 2879-2886.2

APPENDIX

APPENDIX 1: FLAC® CODE

new
call geometry.dat
call functions.dat
set file1=' V1.txt'
set file2=' W (1).txt'
var1
function1
var2
function2
solve
print structures beam
print struct node position
print sxx i=39 j=33,60

"geometry" function:
config
grid 60 60
model mohr
mod null j=30
gen 0,-5 0,0 10,0 10,-5 i=1,61 j=1,30
gen 0,0 0,5 10,5 10,0   i=1,61 j=31,61
group 'layer1' j 1 29
model mohr group 'layer1'
prop density=1.9 bulk=5.33E4 shear=3.20E4 cohesion=100.0 friction=40.0
dilation=10.0 tension=0.0 group 'layer1'
group 'layer2' i 1 60 j 31 60
model mohr group 'layer2'
prop density=1.8 bulk=2.5E4 shear=1.15E4 cohesion=0.0 friction=33.0 dilation=5.0
tension=0.0 group 'layer2'
fix y j 1
fix x i 1
fix x i 61
attach remove
model null i 40 60 j 30 60
def createNodes
 jjGp = 30
 loop iiGp(28,43)
  iNode = iNode+1
  xref = x(iiGp,jjGp)

```
  yref = y(iiGp,jjGp)
  command
   struct node iNode xref,yref
  end_command
 if xref=3
  crossNode = iNode
 end_if
end_loop
iniNode1 = 1
iniNode2 = iNode
iiGp = 40
loop jjGp(32,61)
 iNode = iNode+1
 xref = x(iiGp,jjGp)
 yref = y(iiGp,jjGp)
 command
  struct node iNode xref,yref
 end_command
end_loop
iniNode3 = iniNode2+1
iniNode4 = iNode
end
createNodes
def create_hBeam
 loop iNode(iniNode1,iniNode2-1)
  iNode_ini = iNode
  iNode_end = iNode+1
  command
   struct beam begin node iNode_ini end node iNode_end seg 1 prop 1001
  end_command
 end_loop
end
def create_vBeam
 loop iNode(iniNode3,iniNode4-1)
  iNode_ini = iNode
  iNode_end = iNode+1
  command
   struct beam begin node iNode_ini end node iNode_end seg 1 prop 1002
  end_command
 end_loop
end
struct prop 1001 e 2.58E7 area 0.5 I 0.01041667
struct prop 1002 e 2.58E7 area 0.25 I 0.0013
create_hBeam
```

struct prop 1003 e 2.58E7 area 0.5 I 0.01041667

interface 1 aside from node iniNode2 to node iniNode1 bside from 28,30 to 43,30

interface 1 unglued kn=9.6E6 ks=9.6E6 friction=26.67 tbond=0.0 sbratio=100.0

bslip=off

interface 2 as from node iniNode1 to node 13 bs from 28,31 to 40,31

interface 2 unglued kn=4.04E6 ks=4.04E6 friction=22 tbond=0.0 sbratio=100.0

bslip=off

create_vBeam

interface 3 aside from node iniNode3 to node iniNode4 bside from 40,31 to 40,61

interface 3 unglued kn=4.04E6 ks=4.04E6 friction=22 tbond=0.0 sbratio=100.0

bslip=off

attach aside from 1,30 to 28,30 bside from 1,31 to 28,31

struct beam begin node 13 end node iniNode3 seg 1 prop 1002

set gravity=9.81 ; m/s2

history 999 unbalanced

struct chprop 1003 range 10 10

struct chprop 1003 range 9 9

"function" function:
def var1
array fi(1740)
status=open(file1,0,1)
status=read(fi,(1740))
status=close
loop i(1,1740)
fi(i)=parse(fi(i),1)
endloop
k=0
array element(60,29)
loop m(1,60)
loop n(1,29)
k=k+1
element(m,n)=fi(k)
endloop
endloop
end
def function1
loop r(1,60)
loop s(1,29)
friction(r,s)=element(r,s)
endloop
endloop
end

```
def var2
array fi2(1860)
status=open(file2,0,1)
status=read(fi2,1860)
status=close
loop i(1,1860)
fi2(i)=parse(fi2(i),1)
endloop
l=0
array element2(60,31)
 loop m(1,60)
  loop n(1,31)
   l=l+1
   element2(m,n)=fi2(l)
          endloop
       endloop
end
def function2
t=0
 loop r(1,60)
s=30
t=t+1
if t<60
  loop u(1,31)
s=s+1
if s<61
  friction(r,s)=element2(t,u)
  endloop
 endif
endif
 endloop
end
```

APPENDIX 2: R SOFTWARE CODE

Random variable generation:

```
require(graphics)
require(mvtnorm)
require(truncdist)
iy=0          #Y-coordinate of the interface between layers
clx1=10       #Horizontal correlation length of layer 1 (bottom)
cly1=1        #Vertical correlation length of layer 1 (bottom)
clx2=10       #Horizontal correlation length of layer 2 (top)
cly2=1        #Vertical correlation length of layer 2 (top)
nr=1600    #Number of realizations/simulations
mfi1=tan (0.69813) #Mean of friction angle of layer 1
covfi1=0.1        #cov of friction angle of layer 1
mfi2=tan (0.52359)   #Mean of friction angle of layer 2
covfi2=0.1        #cov of friction angle of layer 2
data=(read.csv('C:/Users/bat05/Desktop/model/New folder/my geometry.csv'))
data=data.frame(N=seq(1,length(data[,1]),1),X=data[,4],Y=data[,5])
#################################################
#Layer 1(top)
#constructing dx and dy matrices for layer 1
layer1=data[data$Y<iy,]
dx1=matrix(rep(NA,length(layer1$X)^2),length(layer1$X),length(layer1$X))
dy1=matrix(rep(NA,length(layer1$X)^2),length(layer1$X),length(layer1$X))
for (i in 1:length(layer1$X)){
 for (j in 1:length(layer1$X)){
   dx1[i,j]=abs(layer1$X[i]-layer1$X[j])
   dy1[i,j]=abs(layer1$Y[i]-layer1$Y[j])
 }
}
#Constructing Correlation matrix for layer 1
cormat1=exp(-(2*dx1/clx1+2*dy1/cly1))
isSymmetric(cormat1)
gau1 <- rmvnorm(mean=rep(0,length(layer1$X)),sig=cormat1,n=nr) #gaussian
variables
Uni1 <- pnorm(gau1) #Now U is uniform
sdfilog1=sqrt(log(1+covfi1^2))
mfilog1=log(mfi1)-sdfilog1^2/2
UU1=matrix(rep(NA,I(length(layer1$X)*nr)),nr,length(layer1$X))
for (i in 1:length(layer1$X)){
 UU1[,i]=qtrunc(Uni1[,i],spec='norm',a=0,b=Inf,mfilog1,sdfilog1)
 UU1[,i]=(atan(UU1[,i])* 180) / (pi)
}
```

```
write.csv(t(UU1),"C:/Users/bat05/Desktop/model/New
folder/rea1_cly_1_clx_10_cov_0.1.csv")
#plot(density(UU1[10,]))
##################################################
#Layer 2(bottom)
#constructing dx and dy matrices for layer 1
layer2=data[data$Y>=iy,]
dx2=matrix(rep(NA,length(layer2$X)^2),length(layer2$X),length(layer2$X))
dy2=matrix(rep(NA,length(layer2$X)^2),length(layer2$X),length(layer2$X))
for (i in 1:length(layer2$X)){
 for (j in 1:length(layer2$X)){
   dx2[i,j]=abs(layer2$X[i]-layer2$X[j])
   dy2[i,j]=abs(layer2$Y[i]-layer2$Y[j])
 }
}
#Constructing Correlation matrix for layer 2
cormat2=exp(-(2*dx2/clx2+2*dy2/cly2))
isSymmetric(cormat2)
gau2 <- rmvnorm(mean=rep(0,length(layer2$X)),sig=cormat2,n=nr) #gaussian
variables
Uni2 <- pnorm(gau2)
sdfilog2=sqrt(log(1+covfi2^2))
mfilog2=log(mfi2)-sdfilog2^2/2
UU2=matrix(rep(NA,I(length(layer2$X)*nr)),nr,length(layer2$X))
for (i in 1:length(layer2$X)){
  UU2[,i]=qtrunc(Uni2[,i],spec="lnorm",a=0,b=Inf,mfilog2,sdfilog2)
  UU2[,i]=(atan(UU2[,i])* 180) / (pi)
 }
write.csv(t(UU2),"C:/Users/bat05/Desktop/model/New
folder/rea2_cly_1_clx_10_cov_0.1.csv")
```

Probability of failure:

data=read.csv("C:/Users/bat05/Desktop/model/1results/from r/out.csv","strings As Factors = FALSE)

pfall=data.frame(NULL)

error=10

p=0.00005 #p=0.5%

N=(196/error)^2*(1-p)/p

N=10000000

meanfc=31 #MPa

meanfy=455 #MPa

d=205 #mm

b=1000 #mm

sdlogfc=sqrt(log(1+0.05^2))

mlogfc=log(meanfc)-sdlogfc^2/2

fc=rlnorm(N,mlogfc,sdlogfc)

sdlogfy=sqrt(log(1+0.05^2))

mlogfy=log(meanfy)-sdlogfy^2/2

fy=rlnorm(N,mlogfy,sdlogfy)

meanlamda_M=1.02

covlamda_M=0.06

sdloglamda_M=sqrt(log(1+covlamda_M^2))

mloglamda_M=log(meanlamda_M)-sdloglamda_M^2/2

lamda_M=rlnorm(N,mloglamda_M,sdloglamda_M)

meanlamda_V= 1.075

covlamda_V=0.1

sdloglamda_V=sqrt(log(1+covlamda_V^2))

mloglamda_V=log(meanlamda_V)-sdloglamda_V^2/2

lamda_V=rlnorm(N,mloglamda_V,sdloglamda_V)

As33=c(1297,1457.5,1470,1500,1600,1700,1800,1900,2000,2100,2326,2516)

As30=c(1523.4,1723.8,1744.3,1785.6,1911.9,2042.00,2176.12,2314.75,2434.05,2582.24,2897.88,3185.17)

As36=c(1166.03,1312.35,1327.21,1357.08,1447.79,1540.23,1634.49,1730.69,1812.43,1912.52,2119.86,2300.83)

cov_M_load=rep(NA,length(data[,1]))

cov_M_res=rep(NA,length(data[,1]))

Mcor=rep(NA,length(data[,1]))

betta=rep(NA,length(data[,1]))

for (i in 1:length(data[,1]))

{

* for (j in 1:length(As33))*

* {*

*   #pf shear*

```
#Load
V_load=rnorm(N,data[i,6],data[i,7]*data[i,6])
#Resistance
kv=1+sqrt(200/d)   #kv<=2
Asmin= 0.26*(2.6/qlnorm(.05,mlogfy,sdlogfy))*b*d #mm2
ro= As[j]/(b*d)
 V_res=0.12*kv*b*d*(100*ro*(fc))^(1/3)/1000 #kN
 vmin=0.035*kv^(3/2)*sqrt(fc)*b*d/1000 #check vload<vmin
#V_diff=V_load-V_res
 pfall[i,1]=length(V_diff[V_diff[]>0])/N
#pf moment
sdlog_mload=sqrt(log(1+data[i,9]^2))
mlog_mload=log(data[i,8])-sdlog_mload^2/2
M_load=rlnorm(N,data[i,8],data[i,8]*data[i,9]) #kN.m
kM=M_load*1e6/(b*d^2*fc)
M_res=(As33[j]/1000000)*0.87*fy*1000*(d/1000)*(0.5+sqrt(0.25-kM/1.134))
#plot(density(M_res),xlim=c(50,200),ylim=c(0,.1))
#lines(density(M_load))
M_diff=M_load-M_res
pfall[i,j]=length(M_diff[M_diff[]>0])/N
cov_M_res[i]=sd(M_res)/mean(M_res)
cov_M_load[i]=sd(M_load)/mean(M_load)
Mcor[i]=cor(M_load,M_res)
betta[i]=(mean(M_res)-
mean(M_load))/(sqrt(sd(M_res)^2+sd(M_load)^22*Mcor[i]*sd(M_res)*sd(M_load))
   }
}
#pf=data.frame(pfM,pfv,pfDR,pfDC,pfDL,pfepR,pfepC,pfepL)
datapf=data.frame(data,pfall,cov_M_res,cov_M_load,mean(M_res),mean(M_load),
Mcor,betta)
write.csv(datapf,C:/Users/bat05/Desktop/model/1results/from r/pf_33.csv)'
```